Journal of Computational Physics **176,** 170–195 (2002)
doi:10.1006/jcph.2001.6974, available online at http://www.idealibrary.com on IDEAL®

# A Numerical Method for the Solution of Electromagnetic Wave Diffraction Problems on Perfectly Conducting Screens

S. K. Kanaun

*Instituto Tecnológico y de Estudios Superiores de Monterrey, Campus Estado de México, División de Ingeniería y Arquitectura, Apdo.Postal 6-3, Módulo de Servicio Postal, Atizapán, 52926, México*
E-mail: kanaoun@campus.cem.itesm.mx

Received February 8, 2001; revised November 5, 2001

A new numerical method is applied to the solution of electromagnetic wave diffraction problems on perfectly conducting screens. The method is based on a special class of Gaussian approximating functions that are used for discretization of the original integral equation of the problem. These functions essentially simplify the construction of the final matrix of the system of linear algebraic equations to which the problem is reduced after the discretization. The method is developed for the solution of 2D and 3D diffraction problems and the numerical results are compared with exact and approximate solutions existent in the literature. The method may be applied to the solution of a wide class of the problems of mathematical physics that can be reduced to boundary pseudo-differential equations. 

*Key Words:* electromagnetic wave diffraction; perfectly conducting screens; Gaussian approximating functions; boundary point method; node mesh generation.

## 1. INTRODUCTION

Numerical methods are widely used for the solution of electromagnetic wave diffraction problems on perfectly conducting surfaces. Usually these problems are first reduced to the solution of the integral equations for the surface current and some variants of the boundary element method (BEM) [1, 2] are applied to the numerical solution of such equations.

For the use of the BEM, the scattering surface should be divided into a finite number of subareas and the unknown functions (the components of the current) are approximated by standard (as a rule polynomial) functions in every subarea. After applying the method of moments or the collocation method, the problem is reduced to the solution of a finite system of linear algebraic equations. The components of the matrix of this system are integrals over the subareas (boundary elements) of the surface. In the problem of scattering on perfectly



0021-9991/02 $35.00

conducting surfaces, these integrals are singular and the complexity of their calculations depends on the type of approximating functions. In a standard BEM, a great portion of the computer time is spent in calculating these integrals. A nontrivial auxiliary problem is dividing an arbitrary surface into a set of boundary elements.

In this study, a new numerical method is applied to the solution of the diffraction problem under consideration. In this method the actual distribution of the surface current is approximated by Gaussian functions located on the planes tangent to the scattering surface at some homogeneous set of surface nodes. The idea to use these functions for the solution of a wide class of integral equations of mathematical physics belongs to V. Maz'ya [3, 4]. The theory of approximation by Gaussian functions was developed in the works of V. Maz'ya [3, 4] and V. Maz'ya and G. Shmidt [5]; the multiresolution analysis based on such functions was proposed in the work of V. Maz'ya and G. Shmidt [6]. These functions were used for the solution of the integral equations of plane elasticity for areas with cracks in [7–9].

The use of these functions for the solution of the integral equations of the diffraction theory has two main advantages. First, the action of the integral operators of the problem on these functions is a combination of few standard functions. The latter may be simply tabulated, kept in the computer memory, and then used for the solution of any diffraction problem. As a result, the time for the calculation of the matrix of the linear system obtained after the discretization of the problem is essentially reduced in comparison with a standard BEM. It is also important that only the coordinates of the surface nodes and the surface orientations at the nodes are necessary for the surface description in the present method. The method was called by V. Maz'ya the boundary point method (BPM) and in the latter the boundary points (nodes) play the role of boundary elements of the conventional BEM. Note that the problem of covering an arbitrary smooth surface by a homogeneous set of nodes is simpler than the detailed description of the geometry of all the boundary elements that is necessary for the application of any traditional BEM to the solution of surface integral equations.

The structure of the article is as follows. In Section 2, the integral equation of the theory of monochromatic electromagnetic wave diffraction on perfectly conducting screens is considered. In Section 3, the BPM is developed for 2D diffraction problems. It is shown that after discretization of the problem using Gaussian approximating functions, the components of the matrix of the linear system are combinations of three standard one-dimensional integrals that depend on three nondimensional parameters (two nondimensional distances and a nondimensional frequency). For small values of the distances these integrals may be simply tabulated and kept in the computer memory. Asymptotic expressions of these integrals for large distances are obtained in the form of well-known special functions. Examples of the numerical solutions of 2D diffraction problems for screens (a circular infinite cylinder, a long plane strip, and a rough surface model) are presented in Section 4.

In Section 5, the method is developed for the 3D case. The action of the integral operator of the 3D diffraction problem on Gaussian approximating functions is obtained in this section. As in the 2D case, the matrix of the linear system of the discretized problem depends only on three one-dimensional integrals. The latter may be tabulated for small values of nondimensional distances and have simple asymptotic expressions for large distances. In Section 6, the numerical solutions of 3D diffraction problems for a perfectly conducting spherical surface and for a plane circular disk are considered. The final conclusions and the

discussion of the area of application of the method are presented in Section 7. A numerical algorithm for generating a homogeneous set of nodes on an arbitrary smooth surface is described in the Appendix.

## 2. THE INTEGRAL EQUATION OF THE PROBLEM OF ELECTROMAGNETIC WAVE DIFFRACTION ON A PERFECTLY CONDUCTING SCREEN

Let a monochromatic electromagnetic wave of frequency $\omega$ propagate through a homogeneous and isotropic medium with dielectric and magnetic permittivities $\varepsilon$ and $\mu$. If the dependence on time $t$ is defined by the factor $e^{i\omega t}$, the amplitudes of electric $\mathbf{E}(x)$ and magnetic $\mathbf{H}(x)$ fields in the medium satisfy the well-known Maxwell equations

$$\begin{aligned} \nabla \times \mathbf{H}(x) &= i\frac{\omega\varepsilon}{c}\mathbf{D}(x), \quad \nabla \cdot \mathbf{D}(x) = 0, \\ \nabla \times \mathbf{E}(x) &= -i\frac{\omega\mu}{c}\mathbf{H}(x), \quad \nabla \cdot \mathbf{H}(x) = 0, \end{aligned} \tag{2.1}$$

where the vectors of electric field $\mathbf{E}(x)$ and electric displacement $\mathbf{D}(x)$ are connected by the equation

$$\mathbf{D}(x) = \varepsilon \mathbf{E}(x).$$

Here $x(x_1, x_2, x_3)$ is a point of the medium with Cartesian coordinates $x_i$, $\nabla = \mathbf{e}_i \frac{\partial}{\partial x_i}$ is the vector gradient, $\mathbf{e}_i$ $(i = 1, 2, 3)$ are unit vectors of the axes $x_i$; summation in respect to repeating indexes is implied. A dot $(\cdot)$ is the scalar product and $(\times)$ is the vector product of vectors and tensors; $c$ is the wave velocity. For simplicity we assume that $\varepsilon = 1$, $\mu = 1$ (vacuum).

Let $\Omega$ be a smooth, perfectly conducting surface embedded in the medium. The electric field $\mathbf{E}(x)$ in the medium with such a surface may be presented in the form [1]

$$\mathbf{E}(x) = \mathbf{E}^0(x) - i\frac{4\pi c}{k_0}\int_\Omega \nabla \times [\nabla \times g(x - x')\mathbf{J}(x')]\, d\Omega'. \tag{2.2}$$

Here $\mathbf{E}^0(x)$ is an incident field that is assumed to be a plane monochromatic wave

$$\mathbf{E}^0(x) = \mathbf{e}\exp(-i\mathbf{k}_0 \cdot x), \quad \mathbf{k}_0 = k_0\mathbf{m}, \quad k_0 = \frac{\omega}{c}, \quad |\mathbf{m}| = 1, \tag{2.3}$$

where $\mathbf{k}_0$ is the wave vector and $\mathbf{e}$ is the polarization vector of this wave. Operator $\nabla$ in Eq. (2.2) acts with respect to point $x$.

The kernel of the integral operator in Eq. (2.2) is the second derivative of Green function $g(x)$ of Helmholtz's operator

$$\nabla g(x) + k_0^2 g(x) = -\delta(x), \quad \Delta = \nabla \cdot \nabla. \tag{2.4}$$

Here $\delta(x)$ is Dirac's delta-function. In the 3D case, $g(x)$ takes the form

$$g(x) = \frac{e^{-ik_0 r}}{4\pi r}, \quad r = |x|, \quad x = x(x_1, x_2, x_3) \tag{2.5}$$

and in the 2D case, $g(x)$ is

$$g(x) = -\frac{i}{4} H_0^{(2)}(k_0 r), \quad r = |x|, \quad x = x(x_1, x_2), \tag{2.6}$$

where $H_0^{(2)}$ is zero-order Hankel function of the second kind.

The density $\mathbf{J}(x)$ of the potential in Eq. (2.2) is the surface current generated on $\Omega$ by incident field $\mathbf{E}^0(x)$. Vector $\mathbf{J}(x)$ belongs to $\Omega$ and thus the following equation holds:

$$\mathbf{n}(x) \cdot \mathbf{J}(x) = 0, \quad x \in \Omega. \tag{2.7}$$

Here $\mathbf{n}(x)$ is a normal vector to the positive side of $\Omega$: for closed surfaces, $\mathbf{n}(x)$ is an external normal; for unclosed surfaces, one of the sides of $\Omega$ should be chosen as the positive one.

The field $\mathbf{E}(x)$ in Eq. (2.2) satisfies Maxwell's equations (2.1) for any current distribution $\mathbf{J}(x)$ on $\Omega$ and the tangent components of this field are continuous on $\Omega$ [1]. The integral term in Eq. (2.2) may be interpreted as the field scattered on $\Omega$. Because the tangent components of total electric field $\mathbf{E}(x)$ should be equal to zero on perfectly conducting surfaces, the boundary condition on $\Omega$ takes the form [1]

$$\mathbf{n}(x) \times \mathbf{E}(x) = 0, \quad x \in \Omega. \tag{2.8}$$

The equation for the surface current follows from Eqs. (2.2) and (2.8) in the form

$$i\frac{4\pi c}{k_0}\mathbf{n}(x) \times \int_\Omega \nabla \times [\nabla \times g(x - x')\mathbf{J}(x')]\, d\Omega' = \mathbf{n}(x) \times \mathbf{E}^0(x), \quad x \in \Omega. \tag{2.9}$$

It should be emphasized that the diffraction problem for screens (unclosed surfaces) cannot be reduced to equations of the second kind by using the classical theory of the potential of a simple or double layer (see the discussion in [10]). The appropriate equation of this problem takes the form of the integral equation (2.9) of the first kind and its kernel is hypersingular. Note that Eq. (2.9) is valid also for closed surfaces but in the latter case the problem may be reduced to the integral equation of the second kind that does not have such a high singularity [1].

Taking into account the equivalence

$$\nabla \times [\nabla \times g(x - x')\mathbf{J}(x')] = [\nabla \otimes \nabla g(x - x')] \cdot \mathbf{J}(x') - \Delta g(x - x')\mathbf{J}(x'), \tag{2.10}$$

where $\otimes$ is the tensor product, one can rewrite Eq. (2.2) in the form

$$\mathbf{E}(x) = \mathbf{E}^0(x) + \mathbf{E}^s(x), \quad \mathbf{E}^s(x) = -i\frac{4\pi c}{k_0}\int_\Omega \mathbf{K}(x - x') \cdot \mathbf{J}(x')\, d\Omega', \tag{2.11}$$

$$\mathbf{K}(x) = \nabla \otimes \nabla g(x) + k_0^2 g(x)\mathbf{1}. \tag{2.12}$$

Here Eq. (2.4) for Green function $g(x)$ is used; $\mathbf{1}$ is the second-rank unit tensor.

Let us introduce projector $\boldsymbol{\theta}(x)$ on the plane tangent to $\Omega$ at point $x$

$$\boldsymbol{\theta}(x) = \mathbf{1} - \mathbf{n}(x) \otimes \mathbf{n}(x), \quad x \in \Omega. \tag{2.13}$$

Because vector $\mathbf{J}(x)$ belongs to $\Omega$, the following equation holds

$$\boldsymbol{\theta}(x)\cdot\mathbf{J}(x)=\mathbf{J}(x),$$

and this is another form of Eq. (2.7). Using projector $\boldsymbol{\theta}(x)$, the boundary condition (2.8) may be rewritten in the following equivalent form:

$$\boldsymbol{\theta}(x)\cdot\mathbf{E}(x)=0,\quad x\in\Omega. \tag{2.14}$$

The equation for $\mathbf{J}(x)$ that follows from Eqs. (2.11) and (2.14) takes the form

$$\begin{gathered} i\frac{4\pi c}{k_0}\int_\Omega \mathbf{U}(x,x')\cdot\mathbf{J}(x')\,d\Omega'=\boldsymbol{\theta}(x)\cdot\mathbf{E}^0(x),\quad x\in\Omega;\\ \mathbf{U}(x,x')=\boldsymbol{\theta}(x)\cdot\mathbf{K}(x-x')\cdot\boldsymbol{\theta}(x'). \end{gathered} \tag{2.15}$$

This equation is totally equivalent to Eq. (2.9). The integral on the left-hand side of Eq. (2.15) has a strong singularity

$$\mathbf{U}(x,x')\sim|x-x'|^{-3}\quad\text{when } x'\to x\in\Omega$$

and should be understood in terms of some regularization. It is possible to demonstrate that for an unclosed surface $\Omega$ with the border $\Gamma$ the regularization formula for this integral has the form

$$\begin{aligned} &\int_\Omega \mathbf{U}(x,x')\cdot\mathbf{J}(x')\,d\Omega'=v.p.\int_\Omega \mathbf{U}(x,x')\cdot[\mathbf{J}(x')-\mathbf{J}(x)]\,d\Omega'\\ &+\boldsymbol{\theta}(x)\cdot\oint_\Gamma \nabla g(x-x')\otimes\boldsymbol{\nu}(x')\,d\Gamma'\cdot\mathbf{J}(x)+k_0^2\int_\Omega g(x-x')\,d\Omega'\mathbf{J}(x),\quad x\in\Omega, \end{aligned} \tag{2.16}$$

where the first integral in the right-hand side is understood as its Cauchy principal value $(v.p)$. Here $\boldsymbol{\nu}(x)$ is the external normal to $\Gamma$ at point $x\in\Gamma$ ($\boldsymbol{\nu}$ is situated in the plane tangent to $\Omega$ at point $x$). For closed surfaces the integral over $\Gamma$ disappears.

If $\Omega$ is an infinite plane $x_3=0$ and $\mathbf{J}(x_1,x_2)$ is a function of **S**-space on $\Omega$, another regularization formula of the operator in Eq. (2.15) may be proposed. (**S**-space consists of infinitely smooth functions that tend to zero at infinity faster than any negative power of $|\bar{x}|$, $\bar{x}=\bar{x}(x_1,x_2)$.) In this case the field $\mathbf{E}^s(x)$ in Eq. (2.11) may be presented as a convolution integral over 3D space and after using Fourier transforms of the integrand functions we get

$$\begin{aligned} \mathbf{E}^s(x)&=-i\frac{4\pi c}{k_0}\int \mathbf{K}(x-x')\cdot\mathbf{J}(\bar{x}')\delta(x'\cdot\mathbf{e}_3)\,dx'\\ &=-i\frac{c}{2k_0\pi^2}\int \bar{\mathbf{K}}(\mathbf{k})\cdot\bar{\mathbf{J}}(\bar{\mathbf{k}})\exp(-i\mathbf{k}\cdot x)\,d\mathbf{k}. \end{aligned} \tag{2.17}$$

Here $\delta(x\cdot\mathbf{e}_3)$ is the delta-function concentrated in the plane $(x_1,x_2)$, $\bar{\mathbf{K}}(\mathbf{k})$ is 3D Fourier transform of tensor $\mathbf{K}(x)$ in Eq. (2.12), and $\bar{\mathbf{J}}(\bar{\mathbf{k}})$ is 2D Fourier transform of function $\mathbf{J}(\bar{x})$, $\mathbf{k}=\mathbf{k}(k_1,k_2,k_3)$ is a vector parameter of Fourier transform, $\bar{\mathbf{k}}=\bar{\mathbf{k}}(k_1,k_2)$,

$$\bar{\mathbf{K}}(\mathbf{k})=\int \mathbf{K}(x)\exp(i\mathbf{k}\cdot x)\,d\mathbf{k}=\frac{1}{k^2-k_0^2}\left(k_0^2\mathbf{1}-\mathbf{k}\otimes\mathbf{k}\right),\quad k=|\mathbf{k}|. \tag{2.18}$$

After integration over coordinate $k_3$ in Eq. (2.17) the scattered field $\mathbf{E}^s(x)$ takes the form

$$\mathbf{E}^s(\bar{x}, x_3) = -i\frac{c}{2k_0\pi}\int \hat{\mathbf{K}}(\bar{\mathbf{k}}, x_3)\cdot\bar{\mathbf{J}}(\bar{\mathbf{k}})\exp(-i\bar{\mathbf{k}}\cdot\bar{x})\,d\bar{\mathbf{k}}, \tag{2.19}$$

$$\hat{\mathbf{K}}(\bar{\mathbf{k}}, x_3)\cdot\bar{\mathbf{J}}(\bar{\mathbf{k}}) = I_0(\bar{k}, x_3)\left(k_0^2\mathbf{1} - \bar{\mathbf{k}}\otimes\bar{\mathbf{k}}\right)\cdot\bar{\mathbf{J}}(\bar{\mathbf{k}}) + I_1(\bar{k}, x_3)(\bar{\mathbf{k}}\cdot\bar{\mathbf{J}}(\bar{\mathbf{k}}))\mathbf{e}_3, \tag{2.20}$$

$$\begin{aligned} I_0(\bar{k}, x_3) &= \frac{1}{\beta(k, k_0)}\exp[-|x_3|\beta(\bar{k}, k_0)],\\ I_1(\bar{k}, x_3) &= isign(x_3)\exp[-|x_3|\beta(\bar{k}, k_0)], \end{aligned} \tag{2.21}$$

$$\beta(\bar{k}, k_0) = \begin{cases} \left(\bar{k}^2 - k_0^2\right)^{1/2}, & \bar{k} \geq k_0\\ i\left(k_0^2 - \bar{k}^2\right)^{1/2}, & \bar{k} < k_0. \end{cases} \tag{2.22}$$

Here $\bar{k} = |\bar{\mathbf{k}}|$, the sign of the square root in Eq. (2.22) for $\beta(\bar{k}, k_0)$ is taken in order to obtain outgoing scattered waves in Eq. (2.19) for $\mathbf{E}^s(\bar{x}, x_3)$. Because $\bar{\mathbf{J}}(\bar{\mathbf{k}})$ is also a function of $\mathbf{S}$-space, the integral in Eq. (2.19) converges absolutely. Thus, in this case the left-hand side of Eq. (2.15) may be presented in the form of the absolutely converging integral

$$\begin{aligned} i\frac{4\pi c}{k_0}\int \mathbf{U}(\bar{x} - \bar{x}')\cdot\mathbf{J}(\bar{x}')\,d\bar{x}' &= i\frac{c}{k_0\pi}\int \mathbf{U}(\bar{\mathbf{k}})\cdot\bar{\mathbf{J}}(\bar{\mathbf{k}})\exp(-i\bar{\mathbf{k}}\cdot\bar{x})\,d\bar{\mathbf{k}},\\ \mathbf{U}(\bar{\mathbf{k}}) = \boldsymbol{\theta}\cdot\hat{\mathbf{K}}(\bar{\mathbf{k}}, x_3)\cdot\boldsymbol{\theta} &= \frac{1}{2\beta(k, k_0)}\left(k_0^2\boldsymbol{\theta} - \bar{\mathbf{k}}\otimes\bar{\mathbf{k}}\right). \end{aligned} \tag{2.23}$$

It follows from this equation that the integral operator in Eq. (2.15) is a pseudo-differential operator with the symbol $\mathbf{U}(\bar{\mathbf{k}})$.

It was proved in [11, 12] that if $k_0 \neq 0$, a unique solution of Eq. (2.15) exists for every smooth right-hand side and belongs to the Hölder space $C^{1/2}(\Omega)$. If $k_0 = 0$ (static field) the homogeneous equation (2.15) has a class of nontrivial solutions that was described in [9, 10]. For the numerical solution of Eq. (2.15) it is useful to take into account the asymptotic behavior of $\mathbf{J}(x)$ near the border $\Gamma$ of $\Omega$. Let $\boldsymbol{\nu}(x_0)$ be the normal to $\Gamma$ and $\boldsymbol{\tau}(x_0)$ be the tangent vector to $\Gamma$ at point $x_0 \in \Gamma$ (vector $\boldsymbol{\nu}(x_0)$ belongs to the plane tangent to $\Omega$ at point $x_0$). Scalar products $\boldsymbol{\nu}(x_0)\cdot\mathbf{J}(x)$ and $\boldsymbol{\tau}(x_0)\cdot\mathbf{J}(x)$ have the asymptotics near $\Gamma$ [12],

$$\boldsymbol{\nu}\cdot\mathbf{J} = O\left(r^{1/2}\right), \quad \boldsymbol{\tau}\cdot\mathbf{J} = O\left(r^{-1/2}\right), \tag{2.24}$$

where $r = |x - x_0|$ is the distance to $\Gamma$ from point $x \in \Omega$ in the direction of $\boldsymbol{\nu}(x_0)$.

## 3. NUMERICAL SOLUTION OF 2D DIFFRACTION PROBLEMS

For the numerical solution of Eq. (2.15) the class of Gaussian approximating functions proposed in [3–6] will be used. Let $u(x)$ be a scalar function in $d$-dimensional space $\mathbf{R}^d$. If $u(x)$ and its first derivative are bounded, $u(x)$ may be approximated by the following series:

$$u(x) \approx u_h(x) = \sum_{m\in\mathbf{Z}^d} u_m\varphi(x - \mathbf{m}h), \quad \varphi(x) = \frac{1}{(\pi D)^{d/2}}\exp\left(-\frac{|x|^2}{Dh^2}\right). \tag{3.1}$$

Here $\mathbf{m} \in \mathbf{Z}^d$ is a $d$-dimensional vector with integer components, $h\mathbf{m}$ are the coordinates of the nodes of this approximation, $h$ is the distance between the neighboring nodes, $u_m =$

$u(h\mathbf{m})$ is the value of the function $u(x)$ at node $x = h\mathbf{m}$, and $D$ is a nondimensional parameter. It is demonstrated in [3–5] that the following estimation holds:

$$|u(x) - u_h(x)| \le ch\|\nabla u\| + |u(x)|R(D), \quad R(D) = O(\exp(-\pi^2 D)). \tag{3.2}$$

Here $\|\nabla u\|$ is the norm in the space of continuous functions, $c = O(1)$. If $h$ is sufficiently small the error of the approximation (3.1) may be made negligible by the appropriate choosing of the parameter $D$ ($D = O(1)$). The properties of this approximation were studied in detail in [3–5].

Let us consider an infinite perfectly conducting cylindrical surface that is parallel to the axis $x_3$, and $\Gamma$ is the intersection of this surface with plane $(x_1, x_2)$ (see Fig. 1). If the wave vector $\mathbf{k}_0$ and the polarization vector $\mathbf{e}$ of the incident field $\mathbf{E}^0(x)$ belong to the plane $(x_1, x_2)$ or if $\mathbf{e}$ is orthogonal to the latter, the diffraction problem is plane and its solution depends only on two coordinates $x_1, x_2$. In the plane case, the electric field $\mathbf{E}(x)$ in the medium may be presented in the form similar to Eq. (2.2),

$$\mathbf{E}(x) = \mathbf{E}^0(x) + \mathbf{E}^s(x), \quad \mathbf{E}^s(x) = -i\frac{4\pi c}{k_0}\int_\Gamma \mathbf{K}(x - x') \cdot \mathbf{J}(x')\, d\Gamma'. \tag{3.3}$$

Here $x = x(x_1, x_2)$, $\mathbf{K}(x)$ has form (2.12), where $\nabla$ is the 2D gradient and $g(x)$ is the 2D Green function in Eq. (2.6). The equation for the surface current $\mathbf{J}(x)$ in the plane case is similar to Eq. (2.15)

$$i\frac{4\pi c}{k_0}\int_\Gamma \mathbf{U}(x, x') \cdot \mathbf{J}(x')\, d\Omega' = \boldsymbol{\theta}(x) \cdot \mathbf{E}^0(x); \quad x \in \Gamma, \tag{3.4}$$

where the left-hand side should be understood in terms of the 2D analogy of regularization (2.16).

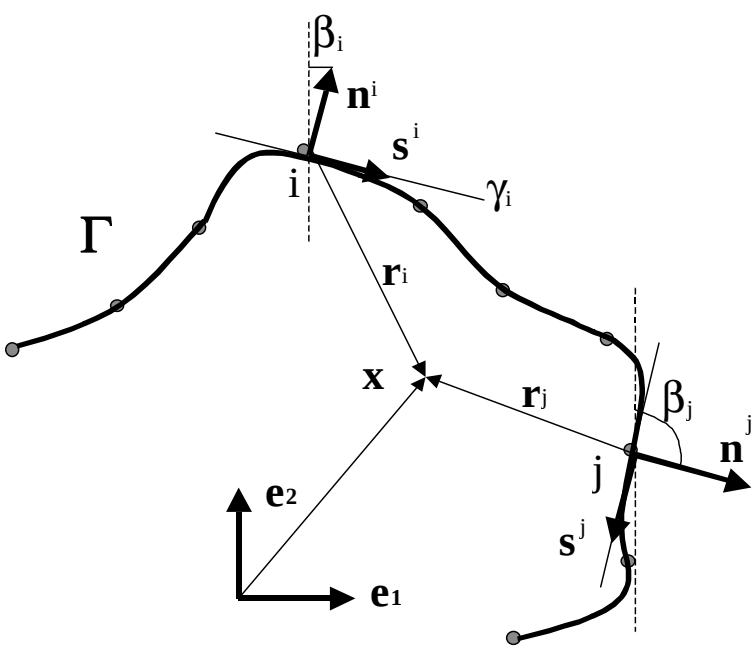


**FIG. 1.** The global $(\mathbf{e}_1, \mathbf{e}_2)$ and local $(\mathbf{s}^{(i)}, \mathbf{n}^{(i)})$ bases in the intersection of a cylindrical surface.

If we introduce the delta-function $\delta(\Gamma)$ concentrated on $\Gamma$, the field $\mathbf{E}^s(x)$ in Eq. (3.3) may be presented in the form

$$\mathbf{E}^s(x) = -i\frac{4\pi c}{k_0}\int \mathbf{K}(x-x')\cdot\mathbf{J}(x')\delta(\Gamma')\,dx', \tag{3.5}$$

where integration is spread over the 2D plane. For the numerical solution of Eq. (3.4) let us choose a set of nodes $x^{(i)}$ on the contour $\Gamma$ with the same distances $h$ between the neighboring nodes and change the potential (3.5) concentrated on $\Gamma$ for the sum of potentials concentrated on the tangent lines $\gamma_i$ to $\Gamma$ at points $x_{(i)}$ (see Fig. 1). Thus, the distribution $\mathbf{J}(x)\delta(\Gamma)$ in Eq. (3.5) is approximated by the sum

$$\mathbf{J}(x)\delta(\Gamma) \approx \sum_i \mathbf{J}^{(i)}\varphi_i(x)\delta(\gamma_i), \tag{3.6}$$

where $\delta(\gamma_i)$ is delta-function concentrated on the tangent line $\gamma_i$ and the function $\varphi_i(x)$ has the form

$$\varphi_i(x) = \varphi_i(x_1, x_2) = \frac{1}{(\pi D)^{1/2}}\exp\left(-\frac{\left(x_1 - x_1^{(i)}\right)^2 + \left(x_2 - x_2^{(i)}\right)^2}{Dh^2}\right). \tag{3.7}$$

After substituting Eq. (3.6) into Eq. (3.5) we go to the following approximation of $\mathbf{E}^s(x)$:

$$\mathbf{E}^s(x) = -i\frac{4\pi c}{k_0}\int \mathbf{K}(x-x')\cdot\mathbf{J}(x')\delta(\Gamma')\,dx' \approx -i4\pi c\sum_i \mathbf{I}^{(i)}(x)\cdot\mathbf{J}^{(i)}, \tag{3.8}$$

$$\mathbf{I}^{(i)}(x) = \frac{1}{k_0}\int \mathbf{K}(x-x')\varphi_i(x')\delta(\gamma_i')\,dx'. \tag{3.9}$$

Let us consider the components $I_{kj}^{(i)}$ of the integral $\mathbf{I}^{(i)}$ in the local coordinate system $(s, z)$ with the origin at the $i$-th node (see Fig. 1):

$$\begin{aligned} I_{kj}^{(i)}(s,z) &= \frac{1}{k_0}\int\int_{-\infty}^{\infty} K_{kj}(s-s', z-z')\varphi(s')\delta(z')\,ds', \\ \varphi(s) &= \frac{1}{(\pi D)^{1/2}}\exp\left(-\frac{s^2}{Dh^2}\right). \end{aligned} \tag{3.10}$$

Here $s$ is the coordinate along the tangent line $\gamma_i$ and $z$ is the coordinate along the normal $\mathbf{n}^{(i)}$ to $\Gamma$ at the $i$-th node. In this local system vector $\mathbf{n}^{(i)}$ has the components $n_s^{(i)} = 0,\ n_z^{(i)} = 1$ and $\delta(\gamma_i) = \delta(z)$. Because $I_{kj}^{(i)}(s, z)$ is a convolution integral, Eq. (3.10) may be rewritten in the form

$$I_{kj}^{(i)}(s,z) = \frac{1}{(2\pi)^2 k_0}\int_{-\infty}^{\infty}\int \tilde{K}_{kj}(k_1,k_2)\tilde{\varphi}(k_1)e^{-i(k_1 s + k_2 z)}\,dk_1\,dk_2. \tag{3.11}$$

Here $\tilde{K}_{kj}(k_1, k_2)$ are the components of the tensor $\bar{\mathbf{K}}(\mathbf{k})$ in Eq. (2.18) if $\mathbf{k}$ is changed for $\bar{\mathbf{k}}$, $\tilde{\varphi}(k_1) = h\exp(-\frac{Dh^2k_1^2}{4})$. After integrating over $k_2$ in Eq. (3.11) we go to an equation similar to Eq. (2.19)

$$\begin{aligned} \frac{1}{2\pi}\int_{-\infty}^{\infty}\bar{\mathbf{K}}(k_1,k_2)\exp(-ik_2 z)\,dk_2 = \frac{1}{2}\Bigg(&\frac{k_0^2}{\beta(k_1,k_0)}\mathbf{1} - \frac{k_1^2}{\beta(k_1,k_0)}\mathbf{s}^{(i)}\otimes\mathbf{s}^{(i)} \\ &+ ik_1 sign(z)\left(\mathbf{s}^{(i)}\otimes\mathbf{n}^{(i)} + \mathbf{n}^{(i)}\otimes\mathbf{s}^{(i)}\right) + \beta(k_1,k_0)\mathbf{n}^{(i)}\otimes\mathbf{n}^{(i)}\Bigg)e^{-|k_1||z|}. \end{aligned} \tag{3.12}$$

Here $\mathbf{s}^{(i)}$, $\mathbf{n}^{(i)}$ are the unit vectors of the axes $s$ and $z$, respectively,

$$\beta(k_1, k_0) = \begin{cases} \left(k_1^2 - k_0^2\right)^{1/2}, & k_1 \geq k_0 \\ i\left(k_0^2 - k_1^2\right)^{1/2}, & k_1 < k_0. \end{cases} \tag{3.13}$$

After substituting Eq. (3.12) into Eq. (3.11) and integrating over $k_1$ we obtain the components of the tensor $\mathbf{I}^{(i)}(s, z)$ in the local system of the $i$-th node. The scalar product $\mathbf{I}^{(i)}(s, z) \cdot \mathbf{J}^{(i)}$ in Eq. (3.8) takes the form

$$\mathbf{I}^{(i)}(s, z) \cdot \mathbf{J}^{(i)} = \frac{2}{\kappa_0 D^{1/2}}[J_{00}(\kappa_0, s, z)\mathbf{1} + J_{11}(\kappa_0, s, z)\mathbf{s}^{(i)} \otimes \mathbf{s}^{(i)} + J_{12}(\kappa_0, s, z)\mathbf{n}^{(i)} \otimes \mathbf{s}^{(i)}] \cdot \mathbf{J}^{(i)},$$

where scalar functions $J_{00}(\kappa_0, s, z)$, $J_{11}(\kappa_0, s, z)$, $J_{12}(\kappa_0, s, z)$ have the forms

$$J_{00}(\kappa_0, s, z) = f_1(\kappa_0, \eta, \zeta) - f_3(\kappa_0, \eta, \zeta), \quad J_{11}(\kappa_0, s, z) = -f_1(\kappa_0, \eta, \zeta), \quad \kappa_0 = k_0 h_1,$$
$$J_{12}(\kappa_0, s, z) = sign(\zeta)\, f_2(\kappa_0, \eta, \zeta), \quad \eta = \frac{s}{h_1}, \quad \zeta = \frac{z}{h_1}, \quad h_1 = \frac{D^{1/2}}{2}h. \tag{3.14}$$

Three functions $f_i(\kappa_0, \eta, \zeta)$ of nondimensional variables in Eq. (3.14) have the forms of the following one dimensional integrals:

$$f_1(\kappa_0, \eta, \zeta) = \frac{1}{2\pi}\int_0^\infty \cos(\kappa\eta)\exp[-\kappa^2 - |\zeta|\beta(\kappa, \kappa_0)]\frac{\kappa^2 d\kappa}{\beta(\kappa, \kappa_0)},$$
$$f_2(\kappa_0, \eta, \zeta) = \frac{1}{2\pi}\int_0^\infty \sin(\kappa\eta)\exp[-\kappa^2 - |\zeta|\beta(\kappa, \kappa_0)]\kappa d\kappa, \tag{3.15}$$
$$f_3(\kappa_0, \eta, \zeta) = \frac{1}{2\pi}\int_0^\infty \cos(\kappa\eta)\exp[-\kappa^2 - |\zeta|\beta(\kappa, \kappa_0)]\beta(\kappa, \kappa_0)\, d\kappa.$$

If $\rho = (\zeta^2 + \eta^2)^{1/2} > 10$ these integrals may be changed with sufficient accuracy for their asymptotic expressions

$$f_1(\kappa_0, \eta, \zeta) \approx -\frac{i\kappa_0}{4\rho}\left[H_1^{(2)}(\kappa_0\rho) - \frac{\kappa_0\eta^2}{\rho}H_2^{(2)}(\kappa_0\rho)\right]\exp\left(-\frac{\kappa_0^2\eta^2}{\rho^2}\right),$$
$$f_2(\kappa_0, \eta, \zeta) \approx -\frac{i\kappa_0^2|\zeta|\eta}{4\rho^2}H_2^{(2)}(\kappa_0\rho)\exp\left(-\frac{\kappa_0^2\eta^2}{\rho^2}\right), \tag{3.16}$$
$$f_3(\kappa_0, \eta, \zeta) \approx \frac{i\kappa_0}{4\rho}\left[H_1^{(2)}(\kappa_0\rho) - \frac{\kappa_0\zeta^2}{\rho}H_2^{(2)}(\kappa_0\rho)\right]\exp\left(-\frac{\kappa_0^2\eta^2}{\rho^2}\right),$$

where $H_1^{(2)}$, $H_2^{(2)}$ are the Hankel functions of the second kind and of order 1 and 2.

The integrals in Eq. (3.15) converge absolutely and for $\rho \leq 10$ they may be calculated numerically, tabulated, and stored in the computer memory.

Let us introduce a global Cartesian coordinate system $(x_1, x_2, x_3)$ with the basis $(\mathbf{e}_1, \mathbf{e}_2, \mathbf{e}_3)$ and the local Cartesian systems $(s, z, x_3)$ with the bases $(\mathbf{s}^{(i)}, \mathbf{n}^{(i)}, \mathbf{e}_3^{(i)})$ at every contour node $x^{(i)}$ (Fig. 1). In the local basis the vector $\mathbf{J}^{(i)}$ in Eq. (3.6) takes the form

$$\mathbf{J}^{(i)} = J_s^{(i)}\mathbf{s}^{(i)} + J_3^{(i)}\mathbf{e}_3^{(i)}. \tag{3.17}$$

The connection between the global and local bases has the form

$$\mathbf{s}^{(i)} = \cos(\beta_i)\mathbf{e}_1 + \sin(\beta_i)\mathbf{e}_2, \quad \mathbf{n}^{(i)} = -\sin(\beta_i)\mathbf{e}_1 + \cos(\beta_i)\mathbf{e}_2, \quad \mathbf{e}_3^{(i)} = \mathbf{e}_3$$

and the connections between the local bases at the $i$-th and $j$-th nodes are

$$\mathbf{s}^{(j)} = \cos(\gamma_{ji})\mathbf{s}^{(i)} + \sin(\gamma_{ji})\mathbf{n}^{(i)}, \quad \mathbf{n}^{(j)} = -\sin(\gamma_{ji})\mathbf{s}^{(i)} + \cos(\gamma_{ji})\mathbf{n}^{(i)}, \quad \gamma_{ji} = \beta_j - \beta_i.$$

Here $\beta_i$ is the angle between unit vectors $\mathbf{e}_2$ and $\mathbf{n}^{(i)}$ (Fig. 1).

Using the last equations and Eqs. (3.8) and (3.14) the scattered field $\mathbf{E}^s(x)$ at arbitrary point $x(x_1, x_2)$ in the global basis may be presented in the form

$$\begin{aligned}
\mathbf{E}^s(x_1, x_2) &\approx -i4\pi c \sum_i \mathbf{I}^{(i)}(x_1, x_2) \cdot \mathbf{J}^{(i)} \\
&= -\sum_i \Psi_{11}\left(r_s^{(i)}, r_n^{(i)}\right) J_s^{(i)}\mathbf{s}^{(i)} + \Psi_{12}\left(r_s^{(i)}, r_n^{(j)}\right) J_s^{(i)}\mathbf{n}^{(i)} + \Psi_3\left(r_s^{(i)}, r_n^{(i)}\right) J_3^{(i)}\mathbf{e}_3 \\
&= -\sum_i \left[\Psi_{11}\left(r_s^{(i)}, r_n^{(i)}\right)\cos\beta_i - \Psi_{12}\left(r_s^{(i)}, r_n^{(j)}\right)\sin\beta_i\right] J_s^{(i)}\mathbf{e}_1 \\
&\quad + \left[\Psi_{11}\left(r_s^{(i)}, r_n^{(j)}\right)\sin\beta_i + \Psi_{12}\left(r_s^{(i)}, r_n^{(i)}\right)\cos\beta_i\right] J_s^{(i)}\mathbf{e}_2 \\
&\quad + \Psi_3\left(r_s^{(i)}, r_n^{(i)}\right) J_3^{(i)}\mathbf{e}_3,
\end{aligned} \tag{3.18}$$

$$\begin{aligned}
\Psi_{11}(r_s, r_n) &= -i\frac{8\pi c}{D^{1/2}} f_3\left(\kappa_0, \frac{r_s}{h_1}, \frac{r_n}{h_1}\right), \\
\Psi_{12}(r_s, r_n) &= i\frac{8\pi c}{D^{1/2}} sign(r_n)\, f_2\left(\kappa_0, \frac{r_s}{h_1}, \frac{r_n}{h_1}\right), \\
\Psi_3(r_s, r_n) &= i\frac{8\pi c}{D^{1/2}}\left[f_1\left(\kappa_0, \frac{r_s}{h_1}, \frac{r_n}{h_1}\right) - f_3\left(\kappa_0, \frac{r_s}{h_1}, \frac{r_n}{h_1}\right)\right].
\end{aligned} \tag{3.19}$$

Here $r_s^{(i)}$ and $r_n^{(i)}$ are the components of the vector $\mathbf{r}^{(i)}$ of arbitrary point $x(x_1, x_2)$ in the local basis $(\mathbf{s}^{(i)}, \mathbf{n}^{(i)})$

$$\begin{gathered}
\mathbf{r}^{(i)} = r_s^{(i)}\mathbf{s}^{(i)} + r_n^{(i)}\mathbf{n}^{(i)}, \quad r_s^{(i)} = \left(x_1 - x_1^{(i)}\right)\cos(\beta_1) + \left(x_2 - x_2^{(i)}\right)\sin(\beta_i), \\
r_n^{(i)} = -\left(x_1 - x_n^{(i)}\right)\sin(\beta_i) + \left(x_2 - x_2^{(i)}\right)\cos(\beta_i).
\end{gathered} \tag{3.20}$$

The tangential component of the field $\mathbf{E}^s(x)$ on $\Gamma$ is approximated by the equation

$$\begin{aligned}
\boldsymbol{\theta}(x) \cdot \mathbf{E}^s(x) &= -i\frac{4\pi c}{k_0}\int_\Gamma \boldsymbol{\theta}(x) \cdot \mathbf{K}(x - x') \cdot \mathbf{J}(x')\, d\Gamma' \\
&\approx -i4\pi c \sum_j \boldsymbol{\theta}(x) \cdot \mathbf{I}^{(j)}(x) \cdot \mathbf{J}^{(j)}, \qquad s \in \boldsymbol{\Gamma}.
\end{aligned} \tag{3.21}$$

The value of this vector at the $i$-th node is presented in the form

$$\theta\left(x^{(i)}\right) \cdot \mathbf{E}^s\left(x^{(i)}\right) = E_s^{(i)}\mathbf{s}^{(i)} + E_3^{(i)}\mathbf{e}_3, \tag{3.22}$$

$$\begin{aligned}
E_s^{(i)} &= -\sum_j \left[\Psi_{11}\left(r_s^{(ij)}, r_n^{(ij)}\right)\cos(\beta_j - \beta_i) - \Psi_{21}\left(r_s^{(ij)}, r_n^{(ij)}\right)\sin(\beta_j - \beta_i)\right] J_s^{(j)}, \\
E_3^{(i)} &= -\sum_j \Psi_3\left(r_s^{(ij)}, r_n^{(ij)}\right) J_3^{(j)}.
\end{aligned} \tag{3.23}$$

Here $(r_s^{(ij)}, r_n^{(ij)})$ are the components of vector $\mathbf{r}^{(ij)}$ that connects the $i$-th and $j$-th nodes, in the local basis of the $j$-th node.

The system of linear algebraic equations for the components $(J_s^{(i)}, J_3^{(i)})$ of the vectors $\mathbf{J}^{(i)}$ follows from the boundary condition (2.14) that should be satisfied at all the nodes (the collocation method). If polarization vector $\mathbf{e}$ of the incident field $\mathbf{E}_0(x)$ belongs to the plane $(x_1, x_2)$ the vector $\mathbf{J}^{(i)}$ in the local basis of the $i$-th node has only $s$-component $(\mathbf{J}^{(i)} = J_s^{(i)}\mathbf{s}^{(i)})$ and the system for $J_s^{(i)}$ takes the form

$$\sum_{j=1}^{M} A_1^{(ij)} J_s^{(j)} = E_s^{0(i)}. \tag{3.24}$$

Here $M$ is the total number of nodes; the components of matrix $A_1$ are

$$A_1^{(ij)} = \Psi_{11}\big(r_s^{(ij)}, r_n^{(ij)}\big)\cos(\gamma_{ji}) - \Psi_{21}\big(r_s^{(ij)}, r_n^{(ij)}\big)\sin(\gamma_{ji}). \tag{3.25}$$

$E_s^{0(i)} = E_s^0(x^{(i)})$ is the $s$-component of the incident field in the $i$-th node.

If the polarization vector of the incident field is orthogonal to the plane $(x_1, x_2)$ $(\mathbf{E}_0(x) = E_3^0(x_1, x_2)\mathbf{e}_3)$ only the components $J_3^{(i)}$ of the vectors $\mathbf{J}^{(i)}$ are not equal to zero $(\mathbf{J}^{(i)} = J_3^{(i)}\mathbf{e}_3)$ and the system for $J_3^{(i)}$ takes the form:

$$\sum_{j=1}^{M} A_2^{(ij)} J_3^{(j)} = E_3^{0(i)}, \quad A_2^{(ij)} = \Psi_3\big(r_s^{(ij)}, r_n^{(ij)}\big), \quad E_3^{0(i)} = E_3^0(x^{(i)}). \tag{3.26}$$

The components of matrixes $A_1$ and $A_2$ in Eqs. (3.24) and (3.26) are expressed via the standard functions $f_i$ $(i = 1, 2, 3)$ in Eqs. (3.15) and (3.16). After solution of Eq. (3.24) or Eq. (3.26) the scattered field at arbitrary point $x$ is to be calculated from Eq. (3.18).

## 4. NUMERICAL RESULTS IN THE 2D CASE

1. Let an incident wave $\mathbf{E}^{(0)}(x)$ with the wave vector $\mathbf{k}_0 = -k_0\mathbf{e}_1$ and the polarization vector $\mathbf{e} = \mathbf{e}_2$ be scattered on a perfectly conducting circular cylindric surface of a unit radius $(a = 1)$ (see Fig. 2). An analytical solution of this problem may be constructed by the method presented in [13].

In this case, only the local components $J_s$ of the current are not equal to zero and the system for $J_s^{(i)}$ (the values of the current at the nodes $x^{(i)}$) has the form of Eq. (3.24). The elements of matrix $A_1$ of this system are expressed via the standard functions $f_i(\kappa_0, \eta, \zeta)$ in Eqs. (3.15) and (3.16). For the interpolation of these functions in the region $(\eta^2 + \zeta^2)^{1/2} < 10$ one has to calculate the integrals in Eq. (3.15) at the nodes of a square interpolating mesh that covers the area $(10 \times 10)$ of variables $(\eta,\ \zeta)$. For $\kappa_0 < 1$ these functions are sufficiently smooth and the step of the mesh may be taken about $\Delta\eta \approx \Delta\zeta \approx 0.2$. For the interpolation in respect to parameter $\kappa_0$ the functions $f_i(\kappa_0, \eta, \zeta)$ should be calculated with the step $\Delta\kappa_0 \approx 0.1$ in the region $\kappa_0 < 1$. Note that parameter $\kappa_0 = k_0 h_1$ should be less then 1 for a sufficient accuracy of the incident field approximation. After constructing these functions, the interpolating data may be kept in the computer memory and used for the solution of any diffraction problem. For large distances $((\eta^2 + \zeta^2)^{1/2} > 10)$ asymptotic expressions

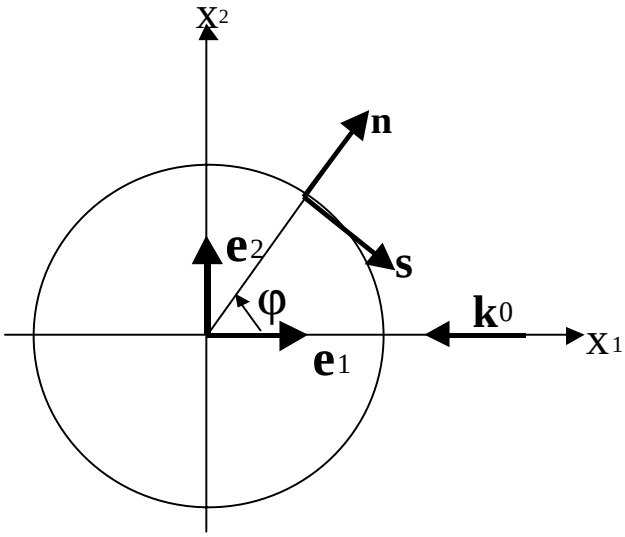


**FIG. 2.** The global ($\mathbf{e}_1$, $\mathbf{e}_2$) and local ($\mathbf{s}$, $\mathbf{n}$) bases in the intersection of a circular cylinder.

(3.16) for $f_i(\kappa_0, \eta, \zeta)$ hold. In 2D case, $D = 2$ is an optimal value of parameter $D$ in the approximation (3.6), (3.7) (see [3–5]).

In the left-hand side of Fig. 3 exact distributions of the surface current moduli $|\mathbf{J}(\varphi)|$ (solid lines) along $\Gamma$ are compared with the numerical solutions for $k_0 a = k_0 = 1; 10$. The nodes are homogeneously distributed along the circle; lines with squares correspond to the number of the nodes $M = 20$ ($h = 0.314$), lines with triangles to $M = 40$ ($h = 0.157$), and lines with dots to $M = 80$ ($h = 0.0785$) for every $k_0 a$. The graphs of the angular distributions of the intensity of the far scattered field $In(\varphi)$ are presented in the right-hand side of Fig. 3:

$$In(\varphi) = (r|\mathbf{E}^s(r, \varphi)|^2)|_{r=100}. \tag{4.1}$$

For $M = 80$ the numerical solutions coincide practically with the exact current distributions. The LU-decomposition method was used for the solution of Eq. (3.24).

2. Let us consider scattering on a plane screen (long strip) ($\Omega = \{x_1 = 0, -1 \le x_2 \le 1, -\infty < x_3 < \infty\}$) when the wave vector $\mathbf{k}_0 = -k_0 \mathbf{e}_1$ of the incident field $\mathbf{E}^{(0)}(x)$ is orthogonal to the strip plane.

a) If the polarization $\mathbf{e}$ of $\mathbf{E}^{(0)}(x)$ is directed along $x_2$-axis ($\mathbf{e} = \mathbf{e}_2$), the current in the strip has only $\mathbf{e}_2$-component

$$\mathbf{J}(x_2) = J_2(x_2)\mathbf{e}_2. \tag{4.2}$$

The distributions of the current moduli $|\mathbf{J}(x)|$, $(x = x_2)$ in the strip and of the scattered field intensity $In(\varphi)$ in the far zone (Eq. (4.1)) are presented in Fig. 4 for $k_0 = 1; 10$ and for various numbers of the nodes in the screen. (Here $k_0$ is in fact a nondimensional wave number $k_0 L$ and $2L = 2$ is the width of the strip.) Lines with squares in Fig. 4 correspond to $M = 20 (h = 0.1)$, lines with triangles to $M = 40 (h = 0.05)$, lines with dots to $M = 60 (h = 0.033)$, and solid lines to $M = 80 (h = 0.025)$. ($\varphi$ is the angle between the

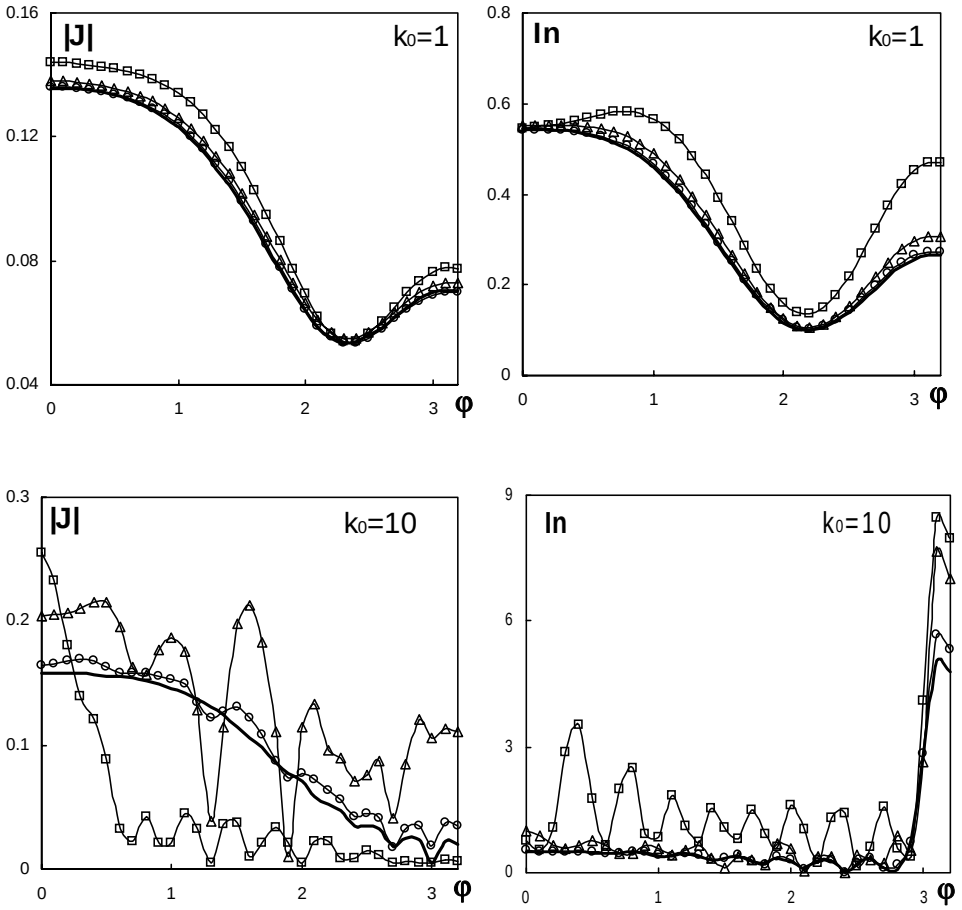


**FIG. 3.** The distributions of the surface current moduli $|\mathbf{J}(x)|$ and the intensity $In(\varphi)$ of the far-scattered field for a circular cylindrical surface of unit radius $a = 1$ for various numbers of surface nodes $M$, lines with □ correspond to $M = 20$, with △ to $M = 40$ and with ○ to $M = 80$, solid lines correspond to the exact solutions, $k_0 = k_0 a$ is nondimentional wave number.

vector of the observation point in the plane $(x_1, x_2)$ and axis $x_2$.) It is seen that the method converges to a limit solution and the latter is practically achieved for $M = 60$.

b) Polarization along the axis of the strip: $\mathbf{e} = \mathbf{e}_3$. For $k_0 = 1; 10$ the convergence of the method may be seen from Fig. 5. The lines with squares in these graphs correspond to $M = 20$, lines with triangles to $M = 40$, lines with dots to $M = 60$, and solid lines to $M = 80$. It is seen from Figs. 4 and 5 that the behavior of the current distributions near the edge of the strip corresponds to the asymptotics of the exact solution given by Eq. (2.24). Long-distance angular distributions of the scattered field intensity $In(\varphi)$ are presented in the left-hand side of Fig. 5.

3. Scattering on a rough surface model:

$$\Omega = \{-10 < x_1 < 10, \quad x_2 = A\cos(\pi x_1), \quad -\infty < x_3 < \infty\}.$$

Let the incident field $\mathbf{E}^0(x)$ have the form

$$\mathbf{E}^0(x) = \mathbf{e}\exp(-i\mathbf{k}_0 \cdot x), \quad \mathbf{k}_0 = \frac{k_0}{2^{1/2}}(\mathbf{e}_1 - \mathbf{e}_2), \quad \mathbf{e} = \frac{1}{2^{1/2}}(\mathbf{e}_1 + \mathbf{e}_2).$$

(The angle between the vectors $\mathbf{k}_0$ and $\mathbf{e}_1$ is $-\pi/4$.)

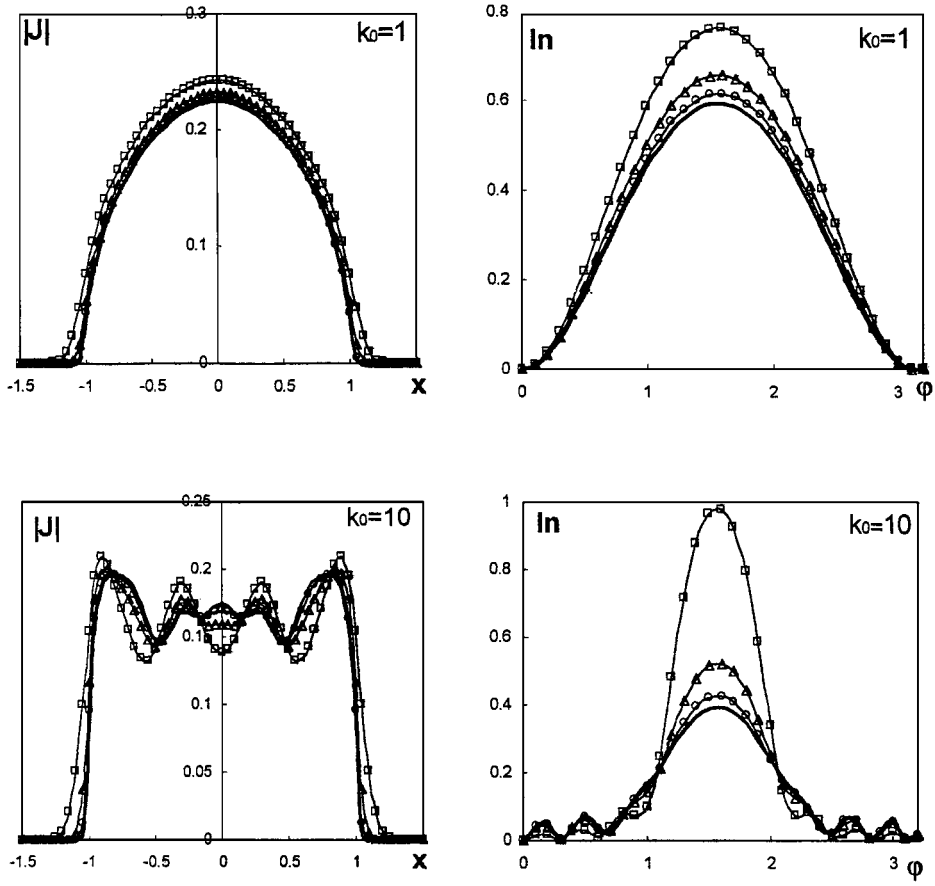


**FIG. 4.** The distributions of the surface current moduli $|\mathbf{J}(x)|$ and the intensity $In(\varphi)$ of the fare scattered field for an infinite strip, the incident field polarization is orthogonal to the axis of the strip. The lines with $\square$ correspond to a number of surface nodes $M = 20$, with $\triangle$ to $M = 40$ and with $\bigcirc$ to $M = 80$.

In Fig. 6 the angle distributions of the scattered field intensity $In(\varphi)$ (Eq. (4.1)) in the far zone for $k_0 = 1; 5$ and various amplitudes $A$ ("roughness") are presented. In these graphs the lines with triangles correspond to $A = 0.1$, lines with rhombs to $A = 0.5$, and lines with dots to $A = 1$. The number of the nodes is $M = 400$ and for such $M$ the limit solutions are practically achieved. The distances $h$ between neighboring nodes along the surfaces are $h = 0.052$ for $A = 0.1$, $h = 0.073$ for $A = 0.5$, and $h = 0.115$ for $A = 1$.

The solid line on the graphs for $k_0 = 5$ corresponds to the so-called Kirchhoff approximation for the case $A = 0.1$. In this approximation the current at every point of $\Omega$ is assumed to be coincident with the current in the perfectly conducting plane tangent to $\Omega$ at this point [14]. It follows from the physical meaning of this approximation that the latter serves better, the smaller is amplitude $A$ (roughness) and the shorter is the wave length of the incident field (larger $k_0$). Qualitatively the behavior of Kirchhoff's approximation in Fig. 6 is similar to the numerical solution but the latter gives five times higher values of the maximum of the scattered field intensity than Kirchoff's approximation predicts. For $A = 0.5$ and $A = 1$ (high roughness) Kirchhoff's approximation gives qualitatively wrong results and cannot be applied for estimating the scattered field intensity.

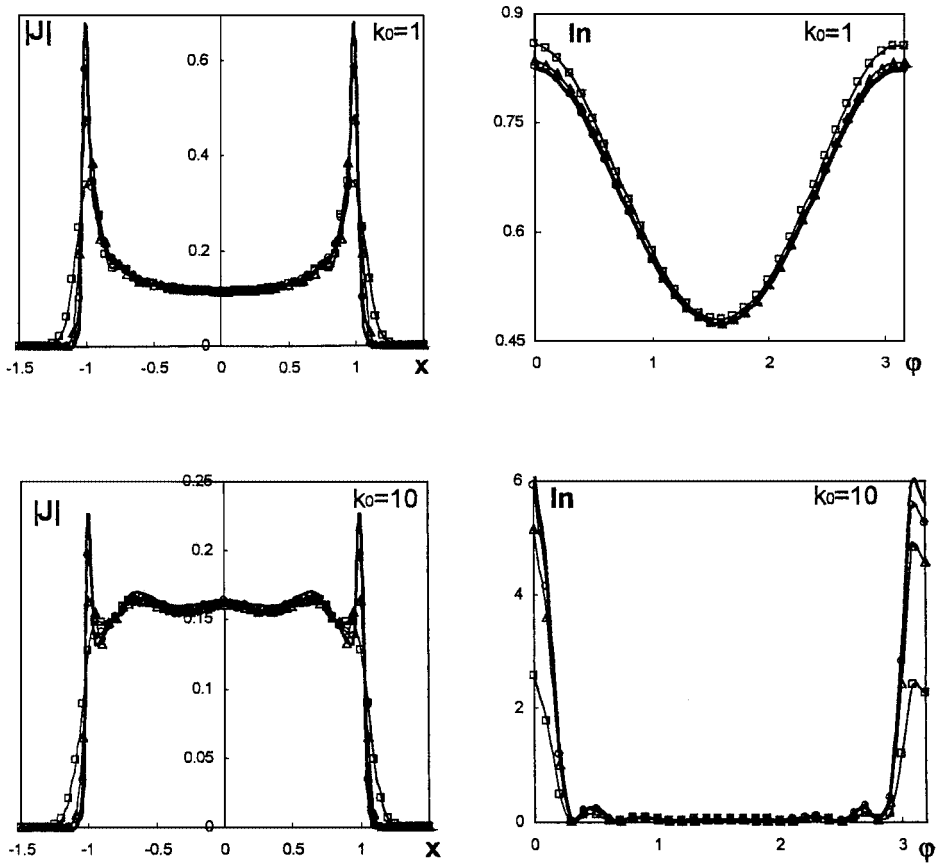


**FIG. 5.** The distributions of the surface current moduli $|\mathbf{J}(x)|$ and the intensity $In(\varphi)$ of the far-scattered field for an infinite strip and various number of surface nodes M, the incident field polarization is parallel to the axis of the strip. The lines with □ correspond to $M = 20$, △ to $M = 40$, ○ to $M = 60$, solid lines to $M = 80$.

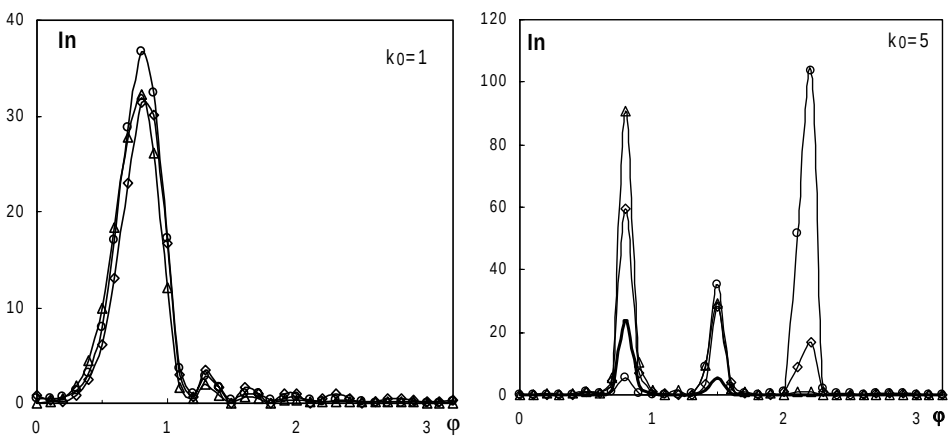


**FIG. 6.** The angular distributions of the intensity $In(\varphi)$ of the far-scattered field for a rough surface model ($x_2 = A\cos(\pi x_1)$) and various values of amplitude $A$. The lines with △ correspond to $A = 0.1$, with ◇ to $A = 0.5$ and with ○ to $A = 1$.

## 5. 3D DIFFRACTION PROBLEMS

In the 3D case, integral equation (2.15) may be presented in the form

$$i\frac{4\pi c}{k_0}\int \mathbf{U}(x,x')\cdot\mathbf{J}(x')\Omega(x')\,dx' = \boldsymbol{\theta}(x)\cdot\mathbf{E}^0(x),\quad x\in\Omega, \tag{5.1}$$

where $\Omega(x)$ is delta-function concentrated on the surface $\Omega$ and integration in this equation is spread over 3D space. Following [3–5], for the application of the BPM, the scattering surface should be covered by a set of nodes $x^{(i)}$ $(i = 1, 2, \ldots, M)$ with approximately the same distances between neighboring nodes. A numerical algorithm for constructing such a set of nodes on an arbitrary smooth surface is presented in the Appendix. Let $\omega_i$ be the tangent plane to $\Omega$ at the $i$-th node. In the BPM the actual current distribution on $\Omega$ is changed for the following sum:

$$\mathbf{J}(x)\Omega(x)\approx\sum_i \mathbf{J}^{(i)}\varphi_i(x)\omega_i(x),\quad \varphi_i(x)=\frac{1}{\pi D}\exp\left(-\frac{|x-x^{(i)}|}{Dh^2}\right). \tag{5.2}$$

Here $\omega_i(x)$ is delta-function concentrated in the plane $\omega_i$ and $\mathbf{J}^{(i)}$ is the vector of this plane. The approximation of the scattered field $\mathbf{E}^s(x)$ in Eq. (2.11) takes the form

$$\mathbf{E}^s(x) = -i\frac{4\pi c}{k_0}\int \mathbf{K}(x-x')\cdot\mathbf{J}(x')\Omega(x')\,dx' \approx -i4\pi c\sum_i \mathbf{I}^{(i)}(x)\cdot\mathbf{J}^{(i)}, \tag{5.3}$$

$$\mathbf{I}^{(i)}(x) = \frac{1}{k_0}\int \mathbf{K}(x-x')\varphi_i(x')\omega_i(x')\,dx'. \tag{5.4}$$

Let us introduce a local Cartesian basis $(\mathbf{e}_1^{(i)}, \mathbf{e}_2^{(i)}, \mathbf{e}_3^{(i)})$ with the origin at the $i$-th node (the unit vector $\mathbf{e}_3^{(i)}$ coincides with the normal $\mathbf{n}^{(i)}$ to $\omega_i$ at point $\mathbf{x}^{(i)}$). In this local coordinate system integral $\mathbf{I}^{(i)}(x)$ takes the form

$$\mathbf{I}^{(i)}(x) = \frac{1}{(2\pi)^3 k_0}\int \bar{\mathbf{K}}(\mathbf{k})\varphi_0(\bar{k})\exp(-i\mathbf{k}\cdot x)\,d\mathbf{k},\quad \varphi_0(\bar{k}) = h^2\exp\left(-\frac{Dh^2\bar{k}^2}{4}\right).$$

Here $\bar{\mathbf{K}}(\mathbf{k})$ has form (2.18), $\mathbf{k}(k_1, k_2, k_3)$ is a vector parameter of the 3D Fourier transform, and $\bar{k}^2 = k_1^2 + k_2^2$. After calculating the integral in this equation by the same way as in Eqs. (2.19) and (3.14), the scalar product $\mathbf{I}^{(i)}(x)\cdot\mathbf{J}^{(i)}$ in Eq. (5.3) in the local basis of the $i$-th node takes the form

$$\begin{aligned}\mathbf{I}^{(i)}(x)\cdot\mathbf{J}^{(i)} = {}& \frac{4}{D\kappa_0}[F_1(\kappa_0,\eta,\zeta)\mathbf{1} + 2F_2(\kappa_0,\eta,\zeta)\boldsymbol{\mu}\otimes\boldsymbol{\mu} \\ & + 2sign(\zeta)F_3(\kappa_0,\eta,\zeta)\mathbf{n}\otimes\boldsymbol{\mu}]\cdot\mathbf{J}^{(i)},\quad \mathbf{n}=\mathbf{e}_3^{(i)},\quad \kappa_0 = k_0h_1, \\ \eta = {}& \frac{1}{h_1}\left(x_1^2+x_2^2\right)^{1/2},\quad \zeta=\frac{x_3}{h_1},\quad \boldsymbol{\mu}=\frac{x_1\mathbf{e}_1^{(i)}+x_2\mathbf{e}_2^{(i)}}{h_1\eta},\quad h_1=\frac{\bar{D}^{1/2}}{2}h.\end{aligned} \tag{5.5}$$

Here the three functions $F_i(\kappa_0, \eta, \zeta)$ are the one-dimensional integrals

$$\begin{aligned} F_1(\kappa_0, \eta, \zeta) &= \frac{1}{8\pi}\int_0^\infty \left[\left(2\kappa_0^2 - \kappa^2\right) J_0(\kappa\eta) - \kappa^2 J_2(\kappa\eta)\right] \\ &\quad \times \exp\left[-k^2 - |\zeta|\beta(\kappa, \kappa_0)\right] \frac{\kappa\, d\kappa}{\beta(\kappa, \kappa_0)}, \\ F_2(\kappa_0, \eta, \zeta) &= \frac{1}{8\pi}\int_0^\infty J_2(\kappa\eta) \exp\left[-k^2 - |\zeta|\beta(\kappa, \kappa_0)\right] \frac{\kappa^3\, d\kappa}{\beta(\kappa, \kappa_0)}, \\ F_3(\kappa_0, \eta, \zeta) &= \frac{1}{8\pi}\int_0^\infty J_1(\kappa\eta) \exp\left[-k^2 - |\zeta|\beta(\kappa, \kappa_0)\right] \kappa^2\, d\kappa, \end{aligned} \tag{5.6}$$

where $\beta(\kappa, \kappa_0)$ is defined in Eq. (2.22), and $J_n(z)$ is the Bessel function of order $n$.

For small values of the arguments $\eta, \zeta (\rho = (\eta^2 + \zeta^2)^{1/2} \le 10)$ these integrals may be simply tabulated and kept in the computer memory. For $\rho > 10$ the following asymptotic expressions for these integrals hold:

$$\begin{aligned} F_1(\kappa_0, \eta, \zeta) &\approx \frac{1}{4\pi\rho^3}\left(-1 + \kappa_0^2\rho^2 - 3i\kappa_0\rho\right) \exp\left(-\frac{\kappa_0^2\eta^2}{\rho^2} - i\kappa_0\rho\right), \\ F_2(\kappa_0, \eta, \zeta) &\approx \frac{\eta^2}{8\pi\rho^2}\left(-\kappa_0^2 + \frac{3i\kappa_0}{\rho} + \frac{3}{\rho^2}\right) \exp\left(-\frac{\kappa_0^2\eta^2}{\rho^2} - i\kappa_0\rho\right), \\ F_3(\kappa_0, \eta, \zeta) &\approx \frac{\eta^2|\zeta|}{8\pi\rho^2}\left(-\kappa_0^2 + \frac{3i\kappa_0}{\rho} + \frac{3}{\rho^2}\right) \exp\left(-\frac{\kappa_0^2\eta^2}{\rho^2} - i\kappa_0\rho\right). \end{aligned} \tag{5.7}$$

As a result, Eq. (5.3) for $\mathbf{E}^s(x)$ takes the form

$$\mathbf{E}^s(x) \approx -i4\pi c \sum_j \mathbf{I}^{(j)}(x) \cdot \mathbf{J}^{(j)} = -\sum_j \sum_{l=1}^{3} \left(\Psi_{l1}\left(\mathbf{r}^{(j)}\right) J_1^{(j)} + \Psi_{l2}\left(\mathbf{r}^{(j)}\right) J_2^{(j)}\right) \mathbf{e}_l^{(j)}, \tag{5.8}$$

$$\begin{aligned} \Psi_{11}\left(\mathbf{r}^{(j)}\right) &= i\frac{16\pi c}{D}\left[F_1\left(\kappa_0, \frac{\rho^{(j)}}{h_1}, \frac{z^{(j)}}{h_1}\right) + 2\left(\frac{r_1^{(j)}}{\rho^{(j)}}\right)^2 F_2\left(\kappa_0, \frac{\rho^{(j)}}{h_1}, \frac{z^{(j)}}{h_1}\right)\right], \\ \Psi_{12}\left(\mathbf{r}^{(j)}\right) &= \Psi_{21}\left(\mathbf{r}^{(j)}\right) = i\frac{32\pi c}{D}\frac{r_1^{(j)} r_2^{(j)}}{\left(\rho^{(j)}\right)^2} F_2\left(\kappa_0, \frac{\rho^{(j)}}{h_1}, \frac{z^{(j)}}{h_1}\right), \\ \Psi_{22}\left(\mathbf{r}^{(j)}\right) &= i\frac{16\pi c}{D}\left[F_1\left(\kappa_0, \frac{\rho^{(j)}}{h_1}, \frac{z^{(j)}}{h_1}\right) + 2\left(\frac{r_2^{(j)}}{\rho^{(j)}}\right)^2 F_2\left(\kappa_0, \frac{\rho^{(j)}}{h_1}, \frac{z^{(j)}}{h_1}\right)\right], \\ \Psi_{31}\left(\mathbf{r}^{(j)}\right) &= i\frac{32\pi c}{D}\frac{r_1^{(j)}}{\rho^{(j)}} sign(z^{(j)}) F_3\left(\kappa_0, \frac{\rho^{(j)}}{h_1}, \frac{z^{(j)}}{h_1}\right), \\ \Psi_{32}\left(\mathbf{r}^{(j)}\right) &= i\frac{32\pi c}{D}\frac{r_2^{(j)}}{\rho^{(j)}} sign\left(z^{(j)}\right) F_3\left(\kappa_0, \frac{\rho^{(j)}}{h_1}, \frac{z^{(j)}}{h_1}\right). \end{aligned} \tag{5.9}$$

$$\mathbf{r}^{(j)} = \mathbf{x} - \mathbf{x}^{(j)} = r_1^{(j)}\mathbf{e}_1^{(j)} + r_2^{(j)}\mathbf{e}_1^{(j)} + z^{(j)}\mathbf{e}_1^{(j)}, \quad \rho^{(j)} = \left[\left(r_1^{(j)}\right)^2 + \left(r_2^{(j)}\right)\right]^{1/2}.$$

Let us introduce a global Cartesian coordinate system $(x_1^0, x_2^0, x_3^0)$ with the basis $(\mathbf{e}_1^{(0)}, \mathbf{e}_2^{(0)}, \mathbf{e}_3^{(0)})$ and a global spherical coordinate system $(\theta, \varphi, r)$ with the same origins. The polar axis of the spherical system is directed along vector $\mathbf{e}_3^{(0)}$ and $\varphi$ is the angle between the vector $\mathbf{e}_1^{(0)}$

and the projection of the vector $x$ on the plane $(x_1^0, x_2^0)$. Let us move vector $\mathbf{n}^{(j)}$ normal to the surface $\Omega$ at the $j$-th node into the origin of the global spherical system using parallel transfer and let the spherical coordinates of the moved vector be $(\theta_j, \varphi_j, 1)$. Local Cartesian basis $(\mathbf{e}_1^{(j)}, \mathbf{e}_2^{(j)}, \mathbf{e}_3^{(j)})$ at the $j$-th node is constructed by parallel transferring the basis $(\mathbf{e}_\theta, \mathbf{e}_\varphi, \mathbf{e}_\tau)$ of the global spherical system at point $(\theta_j, \varphi_j, 1)$ to the $j$-th node $x^{(j)}$

$$\mathbf{e}_1^{(j)} = \mathbf{e}_\theta(\theta_j, \varphi_j, 1), \quad \mathbf{e}_2^{(j)} = \mathbf{e}_\varphi(\theta_j, \varphi_j, 1), \quad \mathbf{e}_3^{(j)} = \mathbf{e}_r(\theta_j, \varphi_j, 1) = \mathbf{n}^{(j)}.$$

In this case the basis vectors of the local and global Cartesian systems are connected by the equations

$$\mathbf{e}_l^j = \sum_{k=1}^{3} Q_{lk}^{(j)} \mathbf{e}_k^{(0)}, \quad \mathbf{e}_l^{(0)} = \sum_{k=1}^{3} \bar{Q}_{lk}^{(j)} \mathbf{e}_k^{(j)}; \tag{5.10}$$

where $Q_{lk}^{(j)}$ and $\bar{Q}_{lk}^{(j)}$ are the components of the matrix $\mathbf{Q}^{(j)}$ and of the matrix $\bar{\mathbf{Q}}^{(j)}$ transposed in respect to $\mathbf{Q}^{(j)}$, respectively. The matrix $\mathbf{Q}^{(j)}$ has the form

$$\mathbf{Q}^{(j)} = \left\| \begin{matrix} \cos\theta_j \cos\varphi_j, & \cos\theta_j \sin\varphi_j, & -\sin\theta_j \\ -\sin\varphi_j, & \cos\varphi_j, & 0 \\ \sin\theta_j \cos\varphi_j, & \sin\theta_j \sin\varphi_j & \cos\theta_j \end{matrix} \right\|. \tag{5.11}$$

As it follows from Eqs. (5.8)–(5.11) in the global Cartesian system, the scattered field $\mathbf{E}^s(x)$ takes the form

$$\mathbf{E}^s(x) \approx -\sum_j \sum_{l=1}^{3} \sum_{k=1}^{3} \left( \Psi_{l1}\left(\mathbf{r}^{(j)}\right) Q_{lk}^{(j)} J_1^{(j)} + \Psi_{l2}\left(\mathbf{r}^{(j)}\right) Q_{lk}^{(j)} J_2^{(j)} \right) \mathbf{e}_k^{(0)}. \tag{5.12}$$

The value of this field in the $i$-th node is presented in the form

$$\begin{gathered} \mathbf{E}^s\left(x^{(i)}\right) = \approx -\sum_j \sum_{l=1}^{3} \sum_{k=1}^{3} \left( \Psi_{l1}\left(\mathbf{r}^{(ij)}\right) T_{lk}^{(ij)} J_1^{(j)} + \Psi_{l2}\left(\mathbf{r}^{(ij)}\right) T_{lk}^{(ij)} J_2^{(j)} \right) \mathbf{e}_k^{(i)}, \\ \mathbf{r}^{(ij)} = \mathbf{x}^{(i)} - \mathbf{x}^{(j)}, \quad T_{lk}^{(ij)} = \sum_{s=1}^{3} Q_{ls}^{(j)} \bar{Q}_{sk}^{(i)}. \end{gathered} \tag{5.13}$$

The system for the components $J_1^{(j)}, J_2^{(j)}$ of the current follows from the boundary conditions (2.14) in the form

$$\sum_{j=1}^{Mn} \left( A_{11}^{ij} J_1^{(j)} + A_{12}^{ij} J_2^{(j)} \right) = E_1^0\left(x^{(i)}\right), \quad \sum_{j=1}^{Mn} \left( A_{21}^{ij} J_1^{(j)} + A_{22}^{ij} J_2^{(j)} \right) = E_2^0\left(x^{(i)}\right). \tag{5.14}$$

Here $E_{1,2}^0(x^{(i)})$ are the tangent components of the incident field $\mathbf{E}^0(x)$ in the local basis of the $i$-th node,

$$A_{mn}^{(ij)} = \sum_{i=1}^{3} \sum_{k=1}^{3} \Psi_{lm}\left(\mathbf{r}^{(ij)}\right) T_{ln}^{(ij)}, \quad m, n = 1, 2. \tag{5.15}$$

After solution of this system, the scattered field $\mathbf{E}^{(s)}$ is to be constructed from Eq. (5.12).

If $M$ is the total number of the nodes, the linear system (5.14) may be rewritten in the canonical form

$$BX = F, \tag{5.16}$$

where the components of the square matrix $B$ of dimensions $(2M \times 2M)$ are

$$\begin{aligned} &B_{ij} = A_{11}^{ij}, \quad i \le M, \quad j \le M; \quad B_{ij} = A_{12}^{i(j-M)}, \quad i \le M, \quad j \le M; \\ &B_{ij} = A_{21}^{(i-M)j}, \quad i > M, \quad j \le M; \quad B_{ij} = A_{22}^{(i-M)(j-M)}, \quad i > M, \quad j > M, \end{aligned} \tag{5.17}$$

and the components of vectors $X$ and $F$ are

$$\begin{aligned} &X_i = J_1^{(i)}, \quad i \le M; \quad X_i = J_2^{(i-M)}, \quad i > M; \\ &F_i = E_1^0(x^{(i)}), \quad i \le M; \quad F_i = E_2^0\big(x^{(i-M)}\big), \quad i > M; \end{aligned} \tag{5.18}$$

$B$ in Eq. (5.16) is a dense matrix with maximal terms concentrated near the main diagonal. For a homogeneous distribution of the nodes on $\Omega$ matrix $B$ is symmetric with the same elements in the main diagonal.

## 6. NUMERICAL RESULTS IN THE 3D CASE

1. Let us consider a spherical surface $\Omega$ of unit radius ($a = 1$). In this case the local basis $(\mathbf{e}_1^{(j)}, \mathbf{e}_2^{(j)}, \mathbf{e}_3^{(j)})$ of the $j$-th node on $\Omega$ coincides with the basis $(\mathbf{e}_\theta, \mathbf{e}_\varphi, \mathbf{e}_\tau)$ of the global spherical system at this node. Let $\mathbf{k}_0 = k_0\mathbf{e}_3^{(0)}$ and $\mathbf{e} = \mathbf{e}_1^{(0)}$ be the wave vector and polarization vector of the incident field $\mathbf{E}^0(x)$, respectively. An analytical solution of this problem may be constructed by the method presented in [13].

For the application of the BPM, a homogeneous set of nodes on $\Omega$ was generated by the algorithm described in the Appendix. In Fig. 7 the dependences of relative error $\Delta$ of the numerical solutions on the number of surface nodes $M$ are presented for $K_0a = 1; 5; 8$,

$$\Delta = \frac{\int_\Omega (|\mathbf{J}_*| - |\mathbf{J}|)^2 \, d\Omega}{\int_\Omega |\mathbf{J}|^2 \, d\Omega}. \tag{6.1}$$

Here $\mathbf{J}_*$ is a numerical solution of Eq. (5.1), and $\mathbf{J}$ is an exact current distribution. In Fig. 8 the distributions of the scattered field intensity $In(\theta, \varphi) = |r\mathbf{E}^s(r, \theta, \varphi)|^2_{r=100}$ in the far zone are given for $\varphi = 0$, $0 \le \theta \le \pi$ and $k_0a = 1; 8$. Solid lines in Fig. 8 correspond to exact solutions, lines with triangles are numerical solutions for $M = 328 (h \approx 0.2)$, lines with rhombs correspond to $M = 508 (h \approx 0.16)$, and lines with dots to $M = 1148 (h \approx 0.1)$. In these calculations parameter $D$ in approximation (5.2) was taken $D = 1.5$.

2. Let us consider the diffraction problem for a thin disk of unit radius ($\Omega = \{(x_1^2 + x_2^2)^{1/2} \le 1, x_3 = 0\}$). The wave vector of the incident field is orthogonal to the disk surface ($\mathbf{k}_0 = k_0\mathbf{e}_3$) and the polarization vector coincides with $\mathbf{e}_1$.

For plane screens the final equations of the method are essentially simplified. The components of the matrixes $A_{mn}$ in Eq. (5.15) take forms

$$A_{mn}^{(ij)} = \Psi_{mn}\big(\mathbf{r}^{(ij)}\big), \quad m, n = 1, 2, \tag{6.2}$$

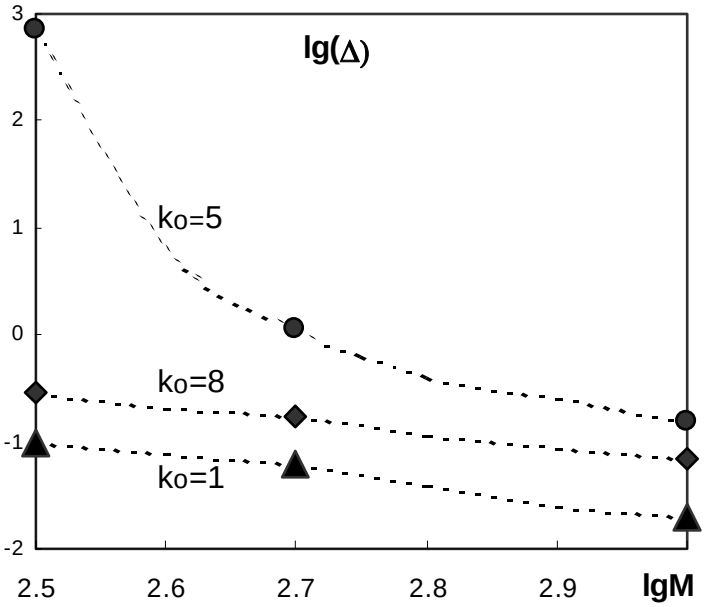


**FIG. 7.** The dependence of the relative integral error $\triangle$ of the numerical calculation of surface current $\mathbf{J}(x)$ in a spherical surface of unit radius $a = 1$ on the number $M$ of surface nodes, the line with triangles corresponds to the relative wave number of the incident field $k_0 a = 1$, with dots to $k_0 a = 5$ and with rhombs to $k_0 a = 8$.

where the functions $\Psi_{mn}(\mathbf{r})$ are defined in Eq. (5.9). These functions are expressed via only two functions $F_1$, $F_2$ in Eq. (5.6) and the latter are in fact the functions of two variables $\kappa_0$ and $\eta(\zeta = 0 \text{ on } \Omega)$.

In Fig. 9 the distributions of the current moduli $|\mathbf{J}(x_1, x_2)|$ along the disk diameters ($|\mathbf{J}(x_1, 0)|$ in the left-hand side and $|\mathbf{J}(0, x_2)|$ in the right-hand side of Fig. 9) are presented for $k_0 a = 1; 10$. Lines with squares correspond to $M = 81$ ($h = 0.2$), lines with triangles to $M = 317 (h = 0.1)$, lines with dots to $M = 797$ ($h = 0.0625$), and solid lines to $M = 1253$ ($h = 0.05$).

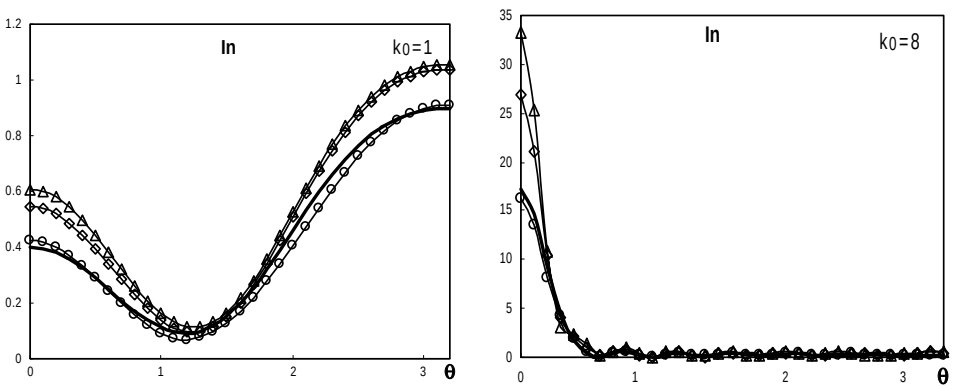


**FIG. 8.** The angle distribution of the intensity $In(\theta)$ of the far-scattered field for a spherical surface of unit radius $a = 1$ with various numbers $M$ of surface nodes, for the wave numbers of incident field $k_0 a = 1; 5$. Lines with triangles correspond to $M = 328$ ($h \approx 0.2$), lines with rhombs to $M = 508$ ($h \approx 0.16$), lines with dots to $M = 1148$ ($h \approx 0.1$), solid lines are exact solutions.

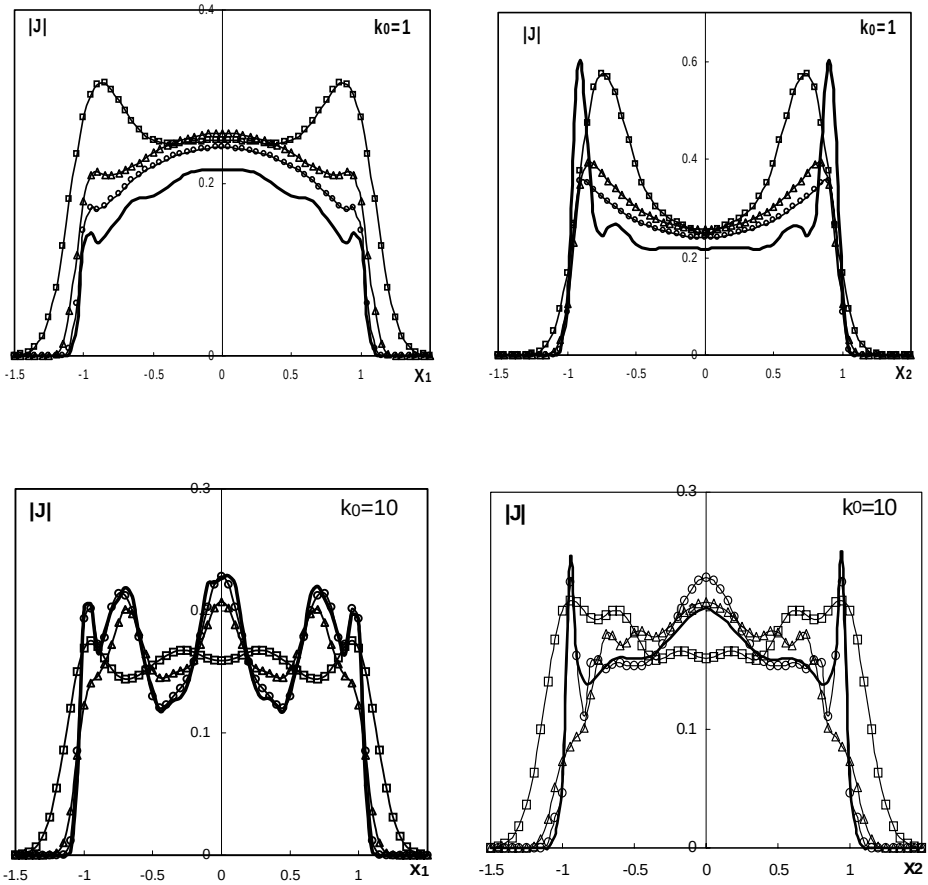


**FIG. 9.** The distribution of the surface current moduli $|\mathbf{J}(x_1, x_2)|$ in a circular disk of unit radius $a = 1$ along its diameter in the direction of axes $x_1, x_2$ for $k_0 a = 1; 10$. Lines with squares correspond to a number of surface nodes $M = 81$ ($h = 0.2$), with triangles to $M = 317$ ($h = 0.1$), with dots to $M = 797$ ($h = 0.0625$) and solid lines to $M = 1253$ ($h = 0.05$).

The angular distributions of scattered field intensity $In(\theta) = |r\mathbf{E}^s(r, \theta, 0)|^2_{r=100}$ in the far zone are presented in Fig. 10.

The solutions of system (5.16) for 3D problems were obtained by the conjugate gradient method [13] with the regularization parameter $\alpha = 0.01$. The number of iterations was taken in order to satisfy the original equation with the precision ~1%:

$$\sum_{i=1}^{2M} \left| \sum_{j=1}^{2M} B_{ij} X_j - F_i \right| < 0.01 \sum_{i=1}^{2M} |F_i|.$$

Note that the method used in this and in the previous sections for the discretization of the 2D and 3D diffraction problems is in essence the collocation method on the basis of the Gaussian approximating functions. It is known that the properties of the systems of linear algebraic equations obtained by the discretization procedure based on the method of moments (MOM) are usually better then the properties of the systems obtained by the collocation method [2]. In some cases the MOM may be also realized on the basis of the Gaussian approximating functions. Let us consider the problem of diffraction on an arbitrary

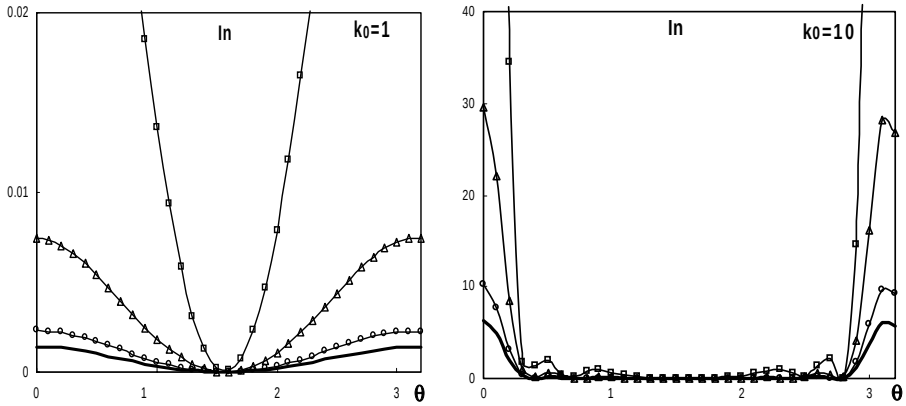


**FIG. 10.** The angular distribution of the intensity $In(\varphi)$ of the far-scattered field for a circular disk for various number of surface nodes and $k_0a = 1; 10$. Lines with squares correspond to a number of surface nodes $M = 81$ ($h = 0.2$), with triangles to $M = 317$ ($h = 0.1$), with dots to $M = 797$ ($h = 0.0625$) and solid lines to $M = 1253$ ($h = 0.05$).

plane area $\Omega$. In this case the integral equation for the surface current takes the form similar to Eq. (5.1)

$$i\frac{4\pi c}{k_0}\int_\Omega \mathbf{U}(x-x')\cdot\mathbf{J}(x')\,dx' = \boldsymbol{\theta}\cdot\mathbf{E}^0(x), \quad x = x(x_1, x_2), \tag{6.3}$$

where $x_1, x_2$ are the Cartesian coordinates in $\Omega$. Fourier transform $\bar{\mathbf{U}}(\mathbf{k})$ of the kernel $\mathbf{U}(x)$ of this equation is given in Eq. (2.23):

$$\bar{\mathbf{U}}(\mathbf{k}) = \frac{1}{2\beta(k, k_0)}\left(k_0^2\mathbf{1} - \mathbf{k}\otimes\mathbf{k}\right), \quad \mathbf{k} = \mathbf{k}(k_1, k_2). \tag{6.4}$$

Let us find the solution of Eq. (6.3) in the form

$$\mathbf{J}(x) = \sum_{j=1}^{M}\mathbf{J}^{(j)}\varphi^j(x), \quad \varphi^j(x) = \frac{1}{D\pi}\exp\left(-\frac{|x-x^j|^2}{Dh}\right), \tag{6.5}$$

where $x^j$ is a set of nodes in the area $\Omega$ with distances $h$ between neighbor nodes. The system for unknown coefficients $\mathbf{J}^{(j)}$ in expansion (6.5) may be obtained by multiplication of both parts of Eq. (6.3) with function $\varphi^j(x)(j = 1, 2, \ldots, M)$ and integration over all the plane $(x_1, x_2)$ (the procedure of the MOM). As a result we go to the following system of linear algebraic equations for vectors $\mathbf{J}^{(j)}$:

$$\sum_{j=1}^{M}\mathbf{A}^{(ij)}\cdot\mathbf{J}^{(j)} = \mathbf{F}^{(i)}, \quad i = 1, 2\ldots, M \tag{6.6}$$

$$\begin{aligned}\mathbf{A}^{(ij)} &= i\frac{4\pi c}{k_0}\int\int\varphi^i(x)\mathbf{U}(x-x')\varphi^j(x')\,dx\,dx' \\ &= i\frac{c}{k_0\pi}\int\bar{\mathbf{U}}(\mathbf{k})\varphi_0^2(k)\exp[-i\mathbf{k}\cdot(x^i - x^j)]\,d\mathbf{k},\end{aligned}$$

$$\varphi_0(k) = h^2\exp\left(-\frac{Dh^2k^2}{4}\right). \tag{6.7}$$

After calculating this integral we obtain the equations for the components of tensors $\mathbf{A}^{(ij)}$ in the forms

$$
\begin{aligned}
A_{11}^{(ij)} &= i\frac{8\pi}{D}\left[F_1\left(\kappa_0, \frac{\rho^{(ij)}}{h_2}, 0\right) + 2\left(\frac{r_1^{(ij)}}{\rho^{(ij)}}\right)^2 F_2\left(\kappa_0, \frac{\rho^{(ij)}}{h_2}, 0\right)\right], \\
A_{12}^{(ij)} &= i\frac{16\pi}{D}\frac{r_1^{(ij)} r_2^{(ij)}}{(\rho^{(ij)})^2} F_2\left(\kappa_0, \frac{\rho^{(ij)}}{h_2}, 0\right), \quad A_{21}^{(ij)} = A_{12}^{(ij)}, \\
A_{11}^{(ij)} &= i\frac{8\pi}{D}\left[F_1\left(\kappa_0, \frac{\rho^{(ij)}}{h_2}, 0\right) + 2\left(\frac{r_2^{(ij)}}{\rho^{(ij)}}\right)^2 F_2\left(\kappa_0, \frac{\rho^{(ij)}}{h_2}, 0\right)\right], \\
\kappa_0 &= k_0 h_2, \quad h_2 = h\left(\frac{D}{2}\right)^{1/2}, \quad \mathbf{r}^{(ij)}\left(r_1^{(ij)}, r_2^{(ij)}\right) = \mathbf{x}^{(i)} - \mathbf{x}^{(j)}, \quad \rho^{(ij)} = |\mathbf{r}^{(ij)}|.
\end{aligned}
\tag{6.8}
$$

Here $F_1$, $F_2$ are the functions defined in Eqs. (5.6) and (5.7). The-right-hand side of Eq. (6.6) takes the form

$$
\mathbf{F}^{(i)} = \int \boldsymbol{\theta} \cdot \mathbf{E}^0(x)\varphi^i(x)\, dx = \frac{h^2}{2D\pi}\sum_{j=1}^{M} \boldsymbol{\theta} \cdot \mathbf{E}^0(x^j) \exp\left(-\frac{|x^i - x^j|^2}{2Dh^2}\right), \tag{6.9}
$$

where the incident field $\mathbf{E}^0(x)$ is approximated by an equation similar to Eqs. (3.1) and (6.5)

$$
\mathbf{E}^0(x) = \frac{1}{D\pi}\sum_{j=1}^{M} \mathbf{E}^0(x^j) \exp\left(-\frac{|x^i - x^j|^2}{Dh^2}\right). \tag{6.10}
$$

Thus, the usage of the Gaussian approximating functions in the framework of the method of moments has the same merit as its usage in the collocation method: it saves the time of calculation of the elements of the matrix of the discretized system. The functions $F_1$, $F_2$ in Eqs. (6.8) for the elements of this matrix have the forms of standard integrals (5.6) and (5.7), and the latter may be previously tabulated and kept in the computer memory. The numerical solutions obtained by the MOM practically coincide with the results of the collocation method except around a small vicinity of the edge of the plane area $\Omega$. Note that the relative error of the both methods is maximum in this region. In order to improve the numerical results in the region of the edges the asymptotic behavior of the solution (2.24) should be taken into account and the numerical algorithm needs modifications. For the calculation of the elastic fields near crack edges, such a modification is discussed in [7–9]. The same scheme may be used for improving the solution of electromagnetic wave diffraction problems in the vicinities of the edges of scattering surfaces.

## 7. CONCLUSION

The use of Gaussian approximating functions proposed in [3, 4] for the solution of the electromagnetic wave diffraction problems on perfectly conducting screens has two main advantages: the simplicity of preparation, of the initial data (the coordinates of surface nodes and surface orientations at the nodes), and a short time for the construction of the matrix of the linear system obtained after the discretization of the problem. The collocation method

or the method of moments may be used for such a discretization. It is assumed that the basic functions of the method ( $f_i(\kappa_0, \zeta, \eta)$ in the 2D case and $F_i(\kappa_0, \zeta, \eta)$ in the 3D case) are previously tabulated and kept in the computer memory.

The accuracy of the method depends on the density of surface nodes. The distances between neighboring nodes should be about $0.05R_c$ in order to have an acceptable accurate solution ($\sim$1%). Here, $R_c$ is a minimal characteristic size of the surface (e.g., a curvature radius, a linear size of the surface, etc.) or a characteristic scale of the incident field. The influence of parameter $D$ in the approximations (3.6), (5.2) on the accuracy of the solution is not essential if $1 < D < 2$. Outside of this region, the convergence of the method with respect to $h$ gets worse. Note that for the calculation of the scattered field in the far zone it is better to choose the smallest values of $D(D \approx 1)$. The convergence with respect to $h$ is faster in this case.

There is a specific difficulty in the application of numerical methods to the solution of the diffraction problems for perfectly conducting screens. In some cases, depending on the shape of the screen and frequency of the incident field, the linear system obtained after discretization of the problem may be ill-posed. For instance, such an ill-posed system may appear for low frequencies (quasistatics) because the original homogeneous integral Eq. (2.15) has nontrivial solutions in the static case (see [11, 12]). Nontrivial solutions of the homogeneous equation (2.15) may exist also for some discrete values of frequencies (see [1], Chapter 6, for details). The application of the LU-decomposition algorithm to the solution of these ill-posed systems gives highly oscillating distributions of the surface current and these oscillations do not disappear when the number of surface nodes increases. These ill-posed problems may be successfully solved using the regularization algorithms described in [15, 16]. But the estimation of the so-called regularization parameter that appears in these algorithms demands additional computational work. It is worth noting that the far scattered fields are not sensitive to the value of the regularization parameter. "Regularized" and "nonregularized" (oscillating) numerical solutions for the current usually give very close results for the intensity of the far scattered field distributions.

The method developed in this study for the solution of the electromagnetic wave diffraction problems may be applied to a wide class of the problems of mathematical physics that are reduced to surface pseudo-differential equations. In particular, the problems of electrostatics, static elasticity, and elasto-plasticity, the problems of elastic wave diffraction on inclusions and cracks, etc., may be successfully solved with the help of the developed version of BPM.

## APPENDIX

Let us consider a rectangular area $S = \{0 \le x_1 \le a, 0 \le x_2 \le b\}$ in the plane $(x_1, x_2)$, where a smooth unique value function $f(x_1, x_2)$ is defined. In order to cover surface $\Omega = \{x_3 = f(x_1, x_2)\}$ by homogeneous set $\mathbf{M}_h$ of nodes with distance $h$ between neighboring nodes, let us introduce a fine regular square mesh on $S$. Step $h_0$ of the fine mesh should be much less than $h(h_0 \ll h)$ and $h_0$ defines the accuracy of the node coordinate definition in the set $\mathbf{M}_h$. Let

$$z_1^{(i)} = h_0(i-1), \quad z_2^{(i)} = h_0(j-1), \quad (i, j, = 1, 2, \ldots) \tag{A.1}$$

be the coordinates of the fine mesh.

Let us choose an arbitrary point $x^{(1)}(x_1^{(1)}, x_2^{(1)})$ inside $S$ as an initial node of set $\mathbf{M}_h$ and introduce the function

$$P(r) = \frac{\left[\left(\frac{r}{h}\right)^n - 1\right]^2}{\alpha + \left(\frac{r}{h}\right)^{2n}}, \quad 0 < \alpha \ll 1; \quad n \gg 1, \tag{A.2}$$

where $\alpha$ is a small parameter and $n$ is a large parameter. This function has a unique minimum ($P = 0$) at point $r = h$ and it tends to 1 when $r \to \infty$ with a speed that depends on $n$. In the calculations, $n = 10$ and $\alpha = 0.1$ were taken.

Point $x^{(2)}$ with coordinates $(x_1^{(2)}, x_2^{(2)})$ is spaced at distance $h$ from $x^{(1)}$, if $x^{(2)}$ provides minimum to the function $P(r^{(1)}(y_1, y_2))$

$$\begin{gathered}\min_{(y_1,y_2)\subset S} P\left(r^{(1)}(y_1, y_2)\right) = P\left(r^{(1)}\left(x_1^{(2)}, x_2^{(2)}\right)\right), \\ r^{(1)}(y_1, y_2) = \left[\left(y_1 - x_1^{(1)}\right)^2 + \left(y_1 - x_1^{(1)}\right)^2 + \left(f(y_1, y_2) - f\left(x_1^{(1)}, x_2^{(1)}\right)\right)^2\right]^{1/2}.\end{gathered} \tag{A.3}$$

In order to find the coordinates of this minimum let us construct matrix $P^{(1)}$ with the components

$$P_{ij}^{(1)} = P\left(r^{(1)}\left(z_1^{(i)}, z_2^{(j)}\right)\right) \tag{A.4}$$

that are the values of $P(r^{(1)}(y_1, y_2))$ at the nodes of the fine mesh in Eq. (A.1). If the minimal element of this matrix has indexes $i_2$, $j_2$, the node $x^{(2)}$ is placed at the point with coordinates $(z_1^{(i_2)}, z_2^{(j_2)})$ according to Eq. (A.1).

In order to obtain the coordinates of the nodes $x^{(3)}, x^{(4)}, \ldots$, let us introduce the function

$$\begin{gathered}W(k, y_1, y_2) = \frac{1}{k}\sum_{i=1}^{k} P\left(r^{(i)}(y_1, y_2)\right), \\ r^{(i)}(y_1, y_2) = \left[\left(y_1 - x_1^{(i)}\right)^2 + \left(y_1 - x_1^{(i)}\right)^2 + \left(f(y_1, y_2) - f\left(x_1^{(i)}, x_2^{(i)}\right)\right)^2\right]^{1/2}.\end{gathered} \tag{A.5}$$

For the calculation of the coordinates of the node $x^{(3)}$ let us take $k = 2$ in this formula. Minimum of $W(2, y_1, y_2)$ is achieved at point $x^{(3)}$ that is at the same distance $h$ from points $x^{(1)}$ and $x^{(2)}$. Let us calculate the elements of the matrix $P^{(2)}$

$$P_{ij}^{(2)} = W\left(2, z_1^{(i)}, z_2^{(j)}\right) \tag{A.6}$$

at the nodes of the fine mesh. The minimal element if this matrix with indexes $i_3$, $j_3$ gives us coordinates $(z_1^{(i_3)}, z_2^{(j_3)})$ of the point $x^{(3)}$ according to Eq. (A.1).

In the same way the coordinates of the node $x^{(i)}$ provide minimum to the function $W(i-1, y_1, y_2)$ and this minimum should be found at the nodes of the fine mesh. The process is stopped if the minimal value of $W(i-1, y_1, y_2)$ becomes more than 1. It means that all the surface $\Omega$ is completely covered by the nodes and any additional node has a neighboring node at the distance that is less than $h$.

The number of terms in Eq. (A.5) grows together with the number of nodes. Therefore, the rate of the calculating process decreases when the number of the constructed node coordinates grows. In order to avoid lengthy calculations, the area $S$ should be divided into several bands (subareas) $S_i$ ($S = \cup S_i$) (e.g., $S_i = \{a_i < x_1 < b_i, 0 < x_2 < b\}$) and the

generation of the nodes may be produced in every band independently. In this case only the nodes in the nearest band with respect to the band where nodes are being constructed should be taken into account in the sum (A.5).

## ACKNOWLEDGMENTS

The work was supported by CNRS (France) and CONACYT (Mexico) and is a part of a joint French–Mexican project. The author thanks Dr. Dominique Jeulin (CMM, Ecole Nacional Superior des Mines de Paris), for the motivation of this study and discussions.

## REFERENCES

1. D. Colton and R. Kress, *Integral Equation Methods in Scattering Theory* (Wiley, New York, 1987).
2. A. F. Peterson, S. L. Ray, and R. Mittra, *Computational Methods for Electro-magnetics* (IEEE Press, New York, 1997).
3. V. Maz'ya, A new approximation method and its applications to the calculation of volume potentials. Boundary point method, in *3. DFG-Koloqium des DFG-Forschungs schwerpunctes 'Randelementmethoden'* (1991).
4. V. Maz'ya, Approximate approximation, in *The Mathematics of Finite Elements and Applications. Highlights 1993*, edited by J. R. Whitman (Wiley, Chichester, 1994), Vol. 77.
5. V. Maz'ya and G. Shmidt, On approximate approximations using Gausian kernels, *IMA J. Numer. Anal*. **16**, 13 (1996).
6. V. Maz'ya and G. Shmidt, Approximate wavelets and the approximation of pseudodifferential operators, *Appl. Comput. Harmonic Anal*. **6**, 287 (1999).
7. S. K. Kanaun, V. Romero, and J. Bernal, A new numerical method for the solution of the second boundary value problem of elasticity for bodies with cracks, *Revista Mexicana de Física* **47**, 309 (2001).
8. S. K. Kanaun and V. Romero, Boundary point method in the dynamic problems of elasticity for plane areas with cracks, *Int. J. Fracture* **111**, L3 (2001).
9. S. K. Kanaun and V. Romero, A numerical method for the solution of the second boundary value problem of elasticity for solids with cracks, *Int. J. Fracture* **107**, L15 (2001).
10. A. S. Il'insky and Yu. G. Smirnov, Integral equation for the problem of wave diffraction at screens, *J. Comm. Tech. Electronics* **39**, 129 (1994).
11. Yu. G. Smirnov, Fredholmness of systems of pseudodifferentioal equations in the problem of diffractions on a bounded screen, *Differential Equations (Differentsial'nye Uravneniya)* **28**, 136 (1992).
12. Yu. G. Smirnov, The solvability of vector integro-differential equations for the problem of the diffraction of an electromagnetic field by screens of arbitrary shape, *Comp. Math. Math. Phys*. **34**, 1265 (1994).
13. Ph. M. Morse and H. Feshbach, *Methods of Theoretical Physics* (McGraw–Hill, New York, 1953).
14. A. G. Voronovich, *Wave Scattering from Rough Surfaces* (Springer-Verlag, Berlin, 1994).
15. V. V. Ivanov, *Methods of Computer Calculations. Handbook* (Naukova Dumka, Kiev, 1986), in Russian.
16. A. N. Tikhonov and V. Ya. Arsenin, *Methods of Solutions of Incorrect Problems* (Nauka, Moscow, 1979), in Russian.